Bifunctional Phagocytic Synapse Enhancers Remodel the Tumor Microenvironment to Overcome Immunosuppression

Valerio Sabatino[1,2*], Cong Tang[3#], Rita C Acúrcio[4#], Ana R Coelho[3], Felix M. Müller[1], Márcia Fontes[5], Wei Ting Khaw[1], Carlos Labão-Almeida[3,13], Derrick R. Hicks[6,7], Wei Yang,[6,7] Aldrin Vasco Vidal[1,13], Irene Sarkar[8], Debarati Shome[8], Mar Cabeza-Cabrerizo[1], Theresa V. Rohm[9], Silvan Fleisch[2], Alexandra Gerber[2], Sabrina A. Hogan[2], Fiona Gerster[2], Deniz Kaymak[2], Stanislav Pantelyushin[10], Johannes vom Berg[10], Lu Li[11], Rogier M. Reijmers[8], Rita Fior[5], David Baker[6,7,12], Helena F. Florindo[4], Gregor Hutter[2], Gonçalo J. L. Bernardes[1,13*]

[1]Yusuf Hamied Department of Chemistry, University of Cambridge, Lensfield Road, CB2 1EW Cambridge, UK.

[2]Department of Biomedicine, Basel University Hospital, Hebelstrasse 20, 4031 Basel, Switzerland.

[3]GIMM - Gulbenkian Institute for Molecular Medicine; Avenida Prof. Egas Moniz, Lisboa, Portugal.

[4]Research Institute for Medicines (iMed.ULisboa), Faculty of Pharmacy Universidade de Lisboa, Lisbon 1649-003, Portugal.

[5]Champalimaud Centre for the Unknown, Champalimaud Foundation Av. Brasília s/n 1400-038 Lisbon PT.

[6]Department of Biochemistry, University of Washington, Seattle, WA, USA.

[7]Institute for Protein Design, University of Washington, Seattle, WA, USA.

[8]Lumicks, Paalbergweg 3, 1105 AG, Amsterdam, Netherlands.

[9]Division of Endocrinology and Metabolism, Department of Medicine, University of California, San Diego, La Jolla, CA 92093, USA.

[10]Institute of Laboratory Animal Science, University of Zurich, Switzerland.

[11]Gator Bio, Inc., Shanghai, China.

[12]Howard Hughes Medical Institute, University of Washington, Seattle, WA, USA.

[13]Translational Chemical Biology Group, Spanish National Cancer Research Centre 26 (CNIO), Madrid 28029, Spain.

Downloaded from aacrjournals.org/cancerres/article-pdf/doi/10.1158/0008-5472.CAN-25-5578/3827263/can-25-5578.pdf by University of Washington user on 07 September 2026

Running Title

Enhancing Phagocytosis for Cancer Immunotherapy

*Corresponding Authors

Valerio Sabatino, Department of Biomedicine, Hebelstrasse 20, 4031 Basel, Switzerland. Email address: valerio.sabatino@unibas.ch;

Gonçalo J. L. Bernardes, Yusuf Hamied Department of Chemistry, Lensfield Road, CB2 1EW Cambridge, UK. Email address: gb453@cam.ac.uk

#These authors contributed equally

Competing Interests statement

V.S. and G.J.L.B. are inventors on a patent application that incorporates the discoveries described in this manuscript [United Kingdom (GB) Patent Application No: 2318879.0]. D.H., W.Y., and D.B. are inventors on a patent application for the de novo PDL1 binder. D.B. is an inventor on a patent application for the de novo EGFR binder. C.T., A.R.C., D.H., W.Y., D.B., and G.J.L.B. have equity in, and are cofounders of Vesto Therapeutic Inc. G.H. and J.v.B. have equity in, and are cofounders of Incephalo Inc. V.S. and G.H have equity in, and are cofounders of GlioCART Inc. All other authors declare no conflict of interest.

Abstract

Current immunotherapies often fail in immunologically “cold”, macrophage-rich tumor microenvironments (TMEs). Multi-targeting approaches that modulate innate-adaptive immune activation represent a promising frontier in cancer immunotherapy. Here, we developed phagocytic synapse enhancers (PSEs), a class of modular immune engagers comprising a high-affinity PD-L1 binder coupled to a macrophage-stimulating peptide, tuftsin. PSEs strengthened effector–target cell interactions and enhanced tumor phagocytosis by bridging tumor PD-L1 to macrophage neuropilin-1 (NRP1), bypassing the classical FcγR-dependent pathways. The PSEs also acted in cis on PD-L1^{+} macrophages, accelerating the endocytosis and lysosomal compartmentalization of surface PD-L1, therefore stripping the immunosuppressive

Downloaded from aacrjournals.org/cancerres/article-pdf/doi/10.1158/0008-5472.CAN-25-5578/3827263/can-25-5578.pdf by University of Washington user on 07 September 2026

checkpoint from the local microenvironment. Beyond physical clearance, PSEs reprogrammed macrophage phenotype and triggered a robust pro-inflammatory cytokine and chemokine response. The lead molecule, ^{long}PSE, and its half-life–extended variant fused to the albumin binding domain, ABD-^{long}PSE, showcased superior efficacy than the macrophage enhancer magrolimab in a syngeneic tumor model of colorectal cancer and an orthotopic model of pancreatic cancer. PSE treatment remodeled the TME by inducing phenotypic changes in the lymphoid and myeloid compartments, together with a reduction of tumor-associated macrophages and regulatory T cells. These findings establish PSEs as bifunctional molecules that complement innate and adaptive immune modulation. The bifunctional design offers a versatile approach for next-generation immunotherapies and provides a blueprint for a plug-and-play platform of immune engagers targeting diverse cancer-associated pathways.

Statement of Significance

Bifunctional immune modulators that simultaneously boost phagocytosis and block immune checkpoints offer a versatile strategy to reprogram the tumor microenvironment and advance next-generation cancer immunotherapy.

Introduction

Immunotherapy has revolutionised the landscape of oncology, yet the immunosuppressive tumor microenvironment (TME) poses a major challenge to the efficacy of traditional treatments. While adaptive immune checkpoint blockade, particularly targeting the PD-1/PD-L1 axis,[1-4] has achieved remarkable clinical success, only a fraction of patients responds to immunotherapy.[5] Immunotherapies frequently fail due to the tumor microenvironment (TME), where myeloid cells, particularly tumor-associated macrophages (TAMs) reprogrammed to promote tumor growth, angiogenesis, and metastasis, drive poor clinical outcomes.[6-11]

Macrophage-targeting approaches include Mϕ depletion, TAM "re-education", antibody-mediated targeting of Mϕ-derived proteins.[12-24] Targeting the CD47/SIRPα "don't eat me" axis with the antibody Magrolimab® marked a major breakthrough for Mϕ-based immunotherapy,[25] however the drug's discontinuation underscores the

Downloaded from aacrjournals.org/cancerres/article-pdf/doi/10.1158/0008-5472.CAN-25-5578/3827263/can-25-5578.pdf by University of Washington user on 07 September 2026

ongoing challenges of using monotherapies. To overcome these multifactorial barriers, there is a critical need for next-generation, multifaceted immunotherapies that can simultaneously disable tumor defenses and actively stimulate localized immune attacks. This is also emphasized by the development of recent multi-targeting approaches.[26-37]

To synergistically disrupt immunosuppression in the tumor microenvironment (TME) and drive robust tumor clearance, we developed Phagocytic Synapse Enhancers (PSEs), a novel class of low-molecular-weight (~15–20 kDa) bifunctional immune engagers. PSEs couple a *de novo* high-affinity PD-L1 binder with the macrophage-activating peptide tuftsin. By simultaneously blocking the PD-L1 inhibitory axis and engaging macrophage neuropilin-1 (NRP1) via tuftsin, PSEs promote a pro-inflammatory phenotype and dramatically strengthen effector-target cell interactions. Notably, our lead constructs, including the half-life-extended ABD-^{long}PSE, outperform Magrolimab® in a syngeneic model of colorectal carcinoma and orthotopic model of pancreatic cancer. Ultimately, PSE treatment remodels the TME by depleting TAMs and regulatory T (Treg) cells, establishing a versatile platform for designing immune engagers against diverse tumor-associated antigens.

Material and Methods

Protein expression and purification. $_{dn}$PDL1, ABD-$_{dn}$PDL1, and $_{dn}$EGFR were provided by the Institute of Protein Design, University of Washington. The recombinant proteins were obtained according to the literature protocol.[38]

The recombinant plasmids for nbPDL1 were transformed into Shuffle T7 competent *E. coli* (New England Biolabs: C3026J; RRID:SCR_013517), and an overnight pre-culture of these were grown in LB media (5 mL) containing ampicillin (50 μg/mL). Pre-cultures were used to inoculate 0.5 L of LB medium containing 50 μg/mL of ampicillin in 2 L flasks to reach an initial OD_{600} of 0.02. These were incubated at 37ºC, 180 rpm until an OD_{600} of 0.8 was reached. At which point, expression was induced upon addition of IPTG (250 μM). The temperature was reduced to 30°C, and the cultures were left to incubate overnight at 180 rpm. The expression media was subsequently collected after centrifugation at 8,000 rpm and 4ºC for 30 min. The pellet was discarded, and the supernatant filtered through a 0.45 μm filter under moderate

Downloaded from aacrjournals.org/cancerres/article-pdf/doi/10.1158/0008-5472.CAN-25-5578/3827263/can-25-5578.pdf by University of Washington user on 07 September 2026

vacuum to remove cellular debris. The supernatant was loaded onto Ni-NTA resin equilibrated with PBS (pH 7.4) and passed over the resin 3x before the bound protein was eluted with an imidazole gradient The imidazole gradient consisted of 10 mM (30 mL), 40 mM (15 mL), 200 mM (5 mL) and 200 mM (10 mL) (all imidazole solutions were in PBS pH 7.4). The fractions were collected and analysed by SDS–PAGE before combining pure protein-containing fractions. Following the combination of fractions, all samples were desalted using HiPrepTM 26/10 Desalting column (Cytiva) eluting with PBS (pH 7.4). Protein concentrations were determined by absorbance at 280 nm using a NanoDrop 2000c UV-Vis spectrophotometer. All protein sequences are reported in the Supplementary Table S1.

Bioconjugation. Fresh batches of cysteine-containing binders in PBS (pH 7.4) were reduced using tris(2-carboxyethyl)phosphine (TCEP) (2.0 equivalents) to remove glutathione and homocysteine capping that occurred during expression, followed by the addition of maleimide linkers (5.0 equivalents) to reach full conjugation, monitored by LC-MS analysis. After conjugation, purification was carried out by SEC using a HiLoad 10/300 Superdex 75 column (Cytiva, Little Chalfont, UK) and PBS (pH 7.4) as an elution buffer.

SDS-PAGE gel. For SDS-PAGE gels, 2 μg of conjugates with SDS dye were loaded onto a Bis-Tris 4–12% Criterion™ XT Bis-Tris Protein Gel, 18 well, (Bio-Rad 3450124) and run with XT-MES buffer at 180 V for 40 min. Proteins were stained with Aquastain (Bulldog Bio AS001000) for 10 min, followed by a 10 min destain in water.

General LC-MS protocols. LC–MS analysis of protein samples was carried out using a Waters SQD2 mass spectrometer using inlet methods A and B, or a Waters Xevo G2-S TOF mass spectrometer using inlet method C, in combination with an Acquity UPLC system with an Acquity UPLC BEH300 C4 column (130 Å, 1.7 μm, 2.1 X 50 mm). The SQD2 mass spectrometer mobile phase consisted of solvent A (99.9% water with 0.1% formic acid), solvent B (71% acetonitrile, 28.9% water, and 0.1% formic acid), and the following gradients were programmed. Inlet method A: 100% A for 2 min, then 100% A to 100% B in 9 min, then 100% B for 5 min, followed by 100% A for 4min. Inlet method B: 100% A for 2min, then 85% A to 100% B in 6 min, then 100% B for 2.5

Downloaded from aacrjournals.org/cancerres/article-pdf/doi/10.1158/0008-5472.CAN-25-5578/3827263/can-25-5578.pdf by University of Washington user on 07 September 2026

min, followed by 85% A for 3.5 min. The Xevo G2-S TOF mass spectrometer mobile phase consisted of solvent A (99.9% water with 0.1% formic acid), solvent B (95% MeCN and 5% water with 0.1% formic acid), and the following gradients were programmed. Inlet method C: 95% A for 0.93 min, then 95% A to 100% B in 4.28 min, then 100% B for 1.04 min, then 100% B to 95% A for 1.04 min. The capillary voltage of the electrospray source for the Waters SQD2 mass spectrometer was 3.0 kV with a cone voltage of 30 V, and the desolvation gas used was nitrogen, with a flow rate of 800 L h−1. For the Waters Xevo G2-S TOF mass spectrometer, the capillary voltage of the electrospray source was 2.0 kV with a cone voltage of 40 V, and the desolvation gas used was nitrogen, with a flow rate of 850 L h−1. The ion series was obtained through integration of the major peaks of the chromatogram. Following this, the total mass spectra were reconstructed using the MaxEnt1 algorithm on the MassLynx software v. 4.1 (RRID:SCR_014271), according to the manufacturer's guidelines.

In vitro studies

Cell culture. All cell lines were purchased from the American Type Culture Collection (ATCC) and were used within 1-30 passages after thawing for all described experiments. RAW 264.7 (RRID:CVCL_0493) and J774A.1 cells (RRID:CVCL_0358) were cultured in Dulbecco's Modified Eagle Medium (DMEM, Gibco) + 10% heat-inactivated foetal bovine serum (FBS, Pan Biotech) with 1% Penicillin/Streptomycin (Gibco). MC-38 (RRID:CVCL_B288) colon carcinoma cells were cultured in DMEM + 10% heat-inactivated FBS, supplemented with HEPES, 1 mM sodium pyruvate, 1X MEM NEAA (#11140-035, Gibco, USA), and 1% pen/strep. U87 cells (RRID:CVCL_0022) were maintained in MEM (#M4655, Sigma-Aldrich, USA) supplemented with 10% inactivated FBS, 1% pen/strep, 1X MEM NEAA (#11140-035, Gibco, USA), 2 mM GlutaMAX-I and 1 mM sodium pyruvate. Cell lines were not independently authenticated beyond the identity provided by the ATCC. Cell lines were cultivated in a humidified incubator at 5% CO_2 and 37°C and tested negative for mycoplasma using a PCR-based assay.

Isolation of peripheral blood mononuclear cells. Peripheral blood leukocytes from healthy donors were obtained from the Blood Donation Center of the University Hospital Basel, Switzerland. Written informed consent was obtained from all

Downloaded from aacrjournals.org/cancerres/article-pdf/doi/10.1158/0008-5472.CAN-25-5578/3827263/can-25-5578.pdf by University of Washington user on 07 September 2026

participants before blood collection. Studies were conducted in accordance with the Declaration of Helsinki and approved by an institutional review board (University Hospital Basel). Peripheral blood mononuclear cells (PBMCs) were isolated using Ficoll Paque-PLUS (GE17-1440-02, Cytiva, Germany) and density centrifugation. After two rounds of ACK-lysis (#A10492-01, Gibco, USA) to remove erythrocytes, PBMCs were washed with PBS. Monocytes were magnetically separated from PBMCs by positive selection using human CD14 MicroBeads (#130-050-201, Miltenyi Biotec, Germany). Primary monocytes were taken fresh after magnetic separation from PBMCs and plated at 0.8 x 10^6 cells per mL in RPMI 1640 (#61870036, Gibco, USA) supplemented with 10% heat-inactivated FBS (#P30-3302, PAN-Biotech, Germany), 5% human serum (#H4522, Sigma-Aldrich, USA), and 25 ng/mL Mϕ colony-stimulating factor (M-CSF, #400-25, PeproTech, USA). After 3-4 d at 37°C and 5% CO_2, the medium was replaced with medium lacking human serum and refreshed every 2-3 d for a maximum of 14 d until use for downstream assays.

Isolation and differentiation of bone-marrow derived Mϕ. After removing all muscles from the legs of ≥8-week-old mice, femur and tibia bones were isolated and flushed out with sterile PBS containing 2% FBS. Bone marrow cells were filtered through a 40 μm strainer (#352340, Falcon) and spun down for 5 min at 500 g. Cell pellets were incubated in Red Cell Lysis Buffer (154 mM NH_4Cl, 10 mM $KHCO_3$, 0.1 mM EDTA) for 3 min and then filled with PBS containing 2% FBS. After a 5-minute centrifugation at 500 g, cells were resuspended in Complete RPMI (10% FBS, Glutamax, Penicillin-Streptomycin (P/S). In the presence of 10-20 ng/mL Recombinant Mouse M-CSF (#576406, BioLegend). Bone marrow cells were differentiated into Bone Marrow-derived Mϕ (BMDMs). Differentiation was started at d0, the same amount of Complete RPMI containing M-CSF was added at d3, and at d6, differentiation medium was removed and exchanged. Macrophages were used on day 6 or 7 for phagocytosis assays, or further polarised for 24 hours to M_1-like (20 ng/mL Interferon gamma (IFNγ), 100 ng/mL LPS) or M_2-like (20 ng/mL IL-4 and IL-13; # 214-14 or #210-13, Peprotech) polarization started at d6 or 7.

Surface Marker analysis of MDMs. Human monocyte-derived macrophages (MDMs) were generated by culturing isolated peripheral blood monocytes in the presence of

Downloaded from aacrjournals.org/cancerres/article-pdf/doi/10.1158/0008-5472.CAN-25-5578/3827263/can-25-5578.pdf by University of Washington user on 07 September 2026

M-CSF (20 ng/mL, PeproTech; Cat# 310-02) for 6 days. Following specific treatments, MDMs were washed once with sterile PBS and gently detached to preserve surface epitope integrity using Accutase (StemCell Technologies; Cat# 07920) for 15-20 minutes at 37 °C. Detached cells were collected, centrifuged at 300 × *g* for 5 minutes, and resuspended in cold FACS buffer (PBS supplemented with 2% FBS and 2 mM EDTA). To exclude dead cells from the analysis, cells were first incubated with a fixable viability dye (Zombie Aqua™ Fixable Viability Kit, BioLegend, Cat# 423101) for 15 minutes at room temperature in the dark, followed by a wash in FACS Buffer. To prevent non-specific antibody binding cells were subsequently incubated with Human TruStain FcX™ (Fc Receptor Blocking Solution, BioLegend; Cat# 422301) for 10 minutes at 4°C. Without washing off the Fc block, cells were stained with a multiplexed panel of fluorophore-conjugated primary antibodies targeting key macrophage surface antigens, including but not limited to: CD45, CD11b, CD274, CD80, CD304, HLA-DR, CD163, and CD206 (see Supplementary Table S2 for comprehensive list of antibody clones, fluorophores, and RRIDs). Staining was performed for 30 minutes at 4°C in the dark. Following incubation, cells were washed twice with FACS buffer to remove unbound antibodies and resuspended in FACS buffer for acquisition.

Cytokine and Chemokine Profiling. Supernatants from cultured macrophages treated with media or PSE constructs for 24 hours were collected and centrifuged to remove debris. Cytokine and chemokine levels were evaluated using the Proteome Profiler Human Cytokine Array Kit (Bio-Techne / R&D Systems; Cat# ARY005B) according to the manufacturer's protocol. Array membranes were imaged via chemiluminescence, and the mean pixel density of each spot was quantified using ImageJ (RRID: SCR_003070). Raw values were background-subtracted and normalized to the internal positive reference spots on each respective array.

Cell binding avidity assays. Tumor cells were attached to poly-L-lysine-coated chips for at least 3h prior to testing on the z-Movi Cell Avidity Analyzer (Lumicks). CellTrace Far Red labelled (ThermoFisher Scientific) Mϕ treated with GRD peptide (50 μM), were flown inside the chip and, in the presence of the PSEs, incubated with the target tumor cells for 3 min prior to application of acoustic force linearly from 0 to 1000pN. Experiments were performed with RAW 264.7 Mϕ and IFNγ treated MC-38 cells. Cell

Downloaded from aacrjournals.org/cancerres/article-pdf/doi/10.1158/0008-5472.CAN-25-5578/3827263/can-25-5578.pdf by University of Washington user on 07 September 2026

detachment was analysed using Ocean software. Experiments and analyses were conducted according to manufacturer recommendations.

PD-L1 competition assays: PD-L1 binding assays were performed with the constitutive PD-L1 expressing tumor cell line MDA-MB-231 (RRID:CVCL_0062). Cells (100,000) were harvested and placed in a U-bottom 96-well plate (TPP, 92697). Checkpoint inhibitors ($_{dn}$PDL1, ^{long}PSE, Atezolizumab) in PBS (100 μL) were added to the wells in a range 0.39-50 nM by serial dilutions together with a fixed concentration of APC-conjugated antibody (aPDL1-APC, Clone: 10F.9G2, RRID:AB_10612935, 1:500 dilution, 133 ng/ml) and incubated for 30min on ice. After staining the cells were harvested and washed twice with MACS buffer. Finally, cells were incubated with DAPI (1mg/mL in DMSO, 1:3,000 dilution) for 10min, washed twice then resuspended in FACS buffer and analysed by flow cytometry (Cytoflex, Beckman Coulter) to determine histograms and the fluorescence intensity of the cells. Data were analysed with FlowJo software (BD Biosciences, RRID:SCR_008520). The IC_{50} for each molecule was determined by Non-linear fit log (inhibitor) vs. response (three parameters) on GraphPad Prism v10 (RRID:SCR_002798).

T-Cell Checkpoint Reporter Assay Functional blockade of the PD-1/PD-L1 axis was evaluated using a cell-based bioluminescent reporter assay. Engineered Jurkat T cells (RRID:CVCL_0065) expressing human PD-1 and an NFAT-driven luciferase reporter were co-cultured with CHO-K1 target cells (RRID:CVCL_0214) stably expressing human PD-L1 and a TCR activator (Promega; Cat# J1250). Co-cultures were treated with titrations of Atezolizumab, Peptide, ABD-$_{dn}$PDL1 or ABD-^{long}PSE. After 8 hours, Bio-Glo™ Luciferase Assay System reagent (Promega; Cat# G7940) was added, and luminescence was measured using a microplate reader Synergy H1 microplate reader (BioTek/Agilent). The EC_{50} for each molecule was determined by Non-linear fit log (inhibitor) vs. response (three parameters) on GraphPad Prism v10 (RRID:SCR_002798).

Immunofluorescence staining assay. MC-38 cells were cultured as mentioned above. According to the type of assay, the cells were plated in a 96-well plate (20,000 cells, 100 μL) and stimulated with IFNγ (20 ng/mL) 24h prior to the assay. After

Downloaded from aacrjournals.org/cancerres/article-pdf/doi/10.1158/0008-5472.CAN-25-5578/3827263/can-25-5578.pdf by University of Washington user on 07 September 2026

stimulation, the fluorescent probes (100 nM) are added to the well and incubated for 1h at 37°C. At the endpoint, the cells are washed with PBS buffer (100 μL x 3) and the cells lifted with TrypLE, centrifuged, resuspended in FACS buffer, and analysed by flow cytometry (Cytoflex, Beckman Coulter) to determine histograms and the fluorescence intensity of the cells. Data were analysed with FlowJo software (BD Biosciences). For confocal microscopy analysis, cells were added to poly-L-lysine-coated 96-well plates, and at the endpoint, the cells were washed with PBS buffer (100 μL x 3) and fixed with 4% PFA. Cells were then imaged with a Leica Stellaris confocal microscope. Data were acquired from a 63× oil immersion objective lens, a green fluorescence channel (ex: 460 ± 10, em: 524 ± 10, acquisition time: 300 ms) or a yellow-orange fluorescence channel (ex: 565 ± 10, em: 578 ± 10).

Characterization of PSEs' binding affinity to PD-L1 by biolayer interferometry. All BLI experiments were performed on an Octet QKe (ForteBio) at 25°C. Proteins for analysis were prepared in sample buffer (PBS, pH 7.4, 0.02% (v/v) Tween-20, and 0.05% (w/v) bovine serum albumin (BSA). The sensorgrams were obtained with a 60 s baseline, 100 s loading, 60 s baseline, 180 s association, and 200 s dissociation. Biotinylated PD-L1-Fc fusion protein (Invitrogen) was diluted to 2 μg/ml in sample buffer and loaded onto Octet Streptavidin biosensors (Sartorius). Individual purified nbPDL1/dnPDL1-conjugates were diluted in sample buffer to between 400 nM and 12.5 nM. Raw data were corrected with double referencing and analysed using Prism v10.0 (GraphPad). The dissociation constants (K_D) for PD-L1 binding were derived from steady-state equilibrium analysis of the sensorgrams using the maximum response observed during association of the PSEs binding to PD-L1 Fc. The binding curves were fitted in Prism to a one-site specific-binding model. Additional kinetic analysis was performed on the sensorgrams to determine k_{on}, k_{off}, and K_D values, using the global analysis model for association kinetics within the Prism9 software.

Characterization of PSEs affinity to NRP1 by BLI. Direct binding interactions between neuropilin 1 (NRP1) and tuftsin derivatives were analysed using a GatorPlus instrument (GatorBio) equipped with SA XT streptavidin biosensors (PN 160011), following the manufacturer's recommendations. All measurements were performed at 30°C with shaking at 1,000 rpm. Biosensors were pre-equilibrated in PBST buffer (PBS

Downloaded from aacrjournals.org/cancerres/article-pdf/doi/10.1158/0008-5472.CAN-25-5578/3827263/can-25-5578.pdf by University of Washington user on 07 September 2026

supplemented with 0.05% Tween-20) for 600 s prior to use. Biotinylated NRP1 (Acro Biosystems, Cat# NR1-H82E3; RRID:SCR_012550) was immobilized at 10 μg mL^{-1} for 30 min at 1,000 rpm as a separate loading step, followed by a 2 min rinse in PBST to remove unbound ligand. For kinetic assays, NRP1-loaded sensors were sequentially exposed to serial dilutions of analyte in PBST. Each binding cycle consisted of a 60 s baseline, 80 s association, and 60 s dissociation step, all conducted at 1,000 rpm. Analyte concentrations were as follows: ABD-^{long}PSE and ^{long}PSE: 100, 50, 25, 12.5, and 6.25 nM; Peptide: 2 μM, 1 μM, 500 nM, 250 nM, 125 nM, and 62.5 nM; dnPDL1 and ABD-dnPDL1: 4 μM, 2 μM, 1 μM, 500 nM, 250 nM, 125 nM, 62.5 nM, 31.25 nM, 15.625 nM, 7.8125 nM, and 3.90625 nM. All analyte solutions were freshly prepared in PBST immediately prior to measurement. Sensorgrams were reference-subtracted and globally fitted to a 1:1 Langmuir binding model using GatorOne software (v2.10.4) to derive kinetic parameters (k_{on}, k_{off}) and the equilibrium dissociation constant (KD).

SPR analysis and characterization of PSEs binding to FcγRs. The SPR method was performed on a Biacore™ 8K+ system (Cytiva), and recombinant receptors bearing a His tag were purchased from AcroBiosystems. Anti His-tag antibodies from the His Capture Kit (Cytiva) were covalently attached to the Series S sensor chip CM5 according to the provider's instructions, with a density of ~10,000 RU. Binding analysis of test samples was performed using the multi-cycle kinetics (MCK) titration method with capture of Fc receptors on the surface of the sensor chip covered by antibody. In the MCK method, each cycle consists of 3 steps: i) injection of the respective Fc receptor, ii) injection of a single concentration of test sample, and iii) injection of regeneration solution. Receptors were diluted in HBS-EP assay buffer (10mM Hepes, 150mM NaCl, 3mM EDTA, 0.05% P20) to a concentration of 0.4 μg/ml and injected into separate channels of the SPR chip before each concentration of test sample using 60-second contact time and a flow rate of 5 μl/min. The average density of receptors achieved 100RU. Test sample serial dilutions were prepared in HBS-EP assay buffer with a concentration range of 10 – 0.01 μM, half-log dilution. The assay running buffer was injected before and after the test sample as a blank (zero concentration of analyte). Test samples were injected from lowest to highest concentration in separate cycles with 60s association and 90s dissociation time, and a flow rate of 30 μl/min. At

Downloaded from aacrjournals.org/cancerres/article-pdf/doi/10.1158/0008-5472.CAN-25-5578/3827263/can-25-5578.pdf by University of Washington user on 07 September 2026

the end of each cycle, a surface is regenerated by injection of 10 mM Glycine, pH 1.5, to remove captured Fc receptor bound to the test sample. After each regeneration, the surface of the chip is flashed in the system with assay running buffer before a new portion of the receptor is captured. Experiments were performed at pH 7.4 for Fc gamma receptors and at pH 6.0 for the neonatal receptor. Four gamma receptors were captured on different channels of a sensor chip, and test samples were analysed on each receptor one after another. The neonatal receptor was immobilized on two channels, and test samples were analysed in parallel. The assay for Fc gamma receptors was performed at pH 7.4, and for the neonatal receptor at pH 6.0.

Integrity of the receptors was evaluated by injection of serial dilutions of the internal control (monoclonal antibody) within each experiment.

Concentration-dependent responses were monitored in the form of sensorgrams, and data were analysed using the Insight Evaluation Software (Cytiva). The response signal of the analyte on the empty chip surface and the response signal of the blank (assay buffer) are subtracted from the total signal, and double-referenced sensorgrams are presented in figures.

Phagocytosis assays. Mϕ were washed with PBS and lifted by mechanical pipetting with cold PBS buffer to avoid enzymatic digestion of the surface receptors. Mϕ were pelleted by centrifugation at 300 × g for 5 min and resuspended in PBS buffer containing CMFDA Green and incubated at 37°C for 30 min. Stained Mϕ (20,000 cells, 100 μL) were added to a 96-well flat-bottom plate (Corning) and incubated in a humidified incubator. Meanwhile, target cells were washed 1x with PBS, detached with TryplE (1 mL), and centrifuged at 300 x g for 5 min. Then, target cells are resuspended in PBS buffer containing Cell Trace Far Red dye (N. C34564, Invitrogen, RRID: SCR_018334) in PBS at 37°C for 30 min, washed with PBS, centrifuged at 300 x g for 5 min, and resuspended in growth medium. The stained tumor cells (100 μL, 20,000 cells) are then added to the 96-well plate containing Mϕ and allowed to attach for 30 min before treatment. Finally, the media was gently removed from the wells, and a solution of PSEs or relative controls (100 μL, 100 nM) in serum-free medium was added to the co-culture and incubated at 37°C for 4 h. *For phagocytosis assays with target cells expressing fluorescent reporters*: macrophages were labelled with Cell Trace Far Red dye.

Downloaded from aacrjournals.org/cancerres/article-pdf/doi/10.1158/0008-5472.CAN-25-5578/3827263/can-25-5578.pdf by University of Washington user on 07 September 2026

PD-L1 Knockout cell line generation. Mouse glioma 261 (GL-261, RRID:CVCL_Y003) cells were provided by A. Fontana (Institute of Experimental Immunology, University of Zurich, Switzerland). Cd274 (PD-L1) targeting was performed using a tracr:crRNA approach (Alt-R CRISPR, iDT) with the same guide design previously reported (5' GTATGGCAGCAACGTCACGA- 3'),[39] but aiming at a non-homologous end joining (NHEJ) approach by omitting the ssDNA template. Ribonucleoproteins (RNPs) with Streptococcus Pyogenes Cas9 (iDT, 1081058) were generated according to the manufacturer's instructions and transfected via electroporation (NEPA21, Nepagene, Japan). After recovery, PD-L1 (CD274) PE (#155404, BioLegend, RRID: AB_2728222) negative cells were sorted into single wells of multiwell plates with conditioned media using BD FACSAria III (BD Biosciences) sorter and individual clones expanded. The knockout clones were confirmed against the parental GL-261 cell line by flow cytometry.

Confocal microscopy for phagocytosis assays. Cells in co-culture were fixed with 4% PFA after 4 h of incubation. Images of fixed cells were taken with a Leica Stellaris 5 confocal microscope. Data were acquired from a 63× oil immersion objective lens at 1x magnification, a green fluorescence channel (ex: 460 ± 20, em: 524 ± 20, acquisition time: 300 ms), and a far-red fluorescence channel (665 ± 40, acquisition time: 400 ms). Two images per well were acquired at the endpoint. Tiles were acquired using a z-stack of 35 μm and images processed by ImageJ (Fiji, RRID:SCR_002285). The number of phagocytised cancer particles and the average MFI were calculated by processing the images on QuPath (Cell detection: Channel 1; requested pixel size: 0.5 μm; Background radius: 8 μm; sigma: 1.5; minimum area: 10 μm; maximum area 400 μm^2; Threshold: 13.49. Channel 2: Threshold: 22.78).

Flow cytometric analysis for phagocytosis assays. Quantitative analysis of the phagocytosis assay was performed by flow cytometry (Cytoflex, Beckman Coulter). The phagocytosis assay was stopped at the endpoint by adding cold FACS buffer to the wells and placing the 96-well plate on ice. The cells were transferred to an Eppendorf tube and acquired. FlowJo software (RRID:SCR_008520) was used to gate on intact cells and single cells to determine the percentage of double positives, Mϕ $PE^+APC\text{-}750^+$. Phagocytic index is calculated by gating on Mϕ only and analysing the

Downloaded from aacrjournals.org/cancerres/article-pdf/doi/10.1158/0008-5472.CAN-25-5578/3827263/can-25-5578.pdf by University of Washington user on 07 September 2026

ratio of $PE^+APC\text{-}750^+$ Mϕ against total Mϕ (PE^+ Mϕ + $PE^+APC\text{-}750^+$ Mϕ). Data analysis was performed on Prism v10 (GraphPad, USA). Note: CMFDA was too bright on the FITC channel, we used PE channel to gate Mϕ as CMFDA green is co-emitting in the PE channel.

Imaging flow cytometry analysis. THP-1 cells (RRID:CVCL_0006) were differentiated to Mϕ with PMA (50 nM) for 48h in a cell culture-treated 24-well plate. After differentiation, PD-L1 expression was induced for 24h with IFNγ (20 ng/ml), and cells were treated with the PSEs or relative controls and incubated at 37°C. At the end of the time point, cells were washed three times with PBS and stained for PD-L1 with aPD-L1-APC (BioLegend, #329707, RRID:AB_940360) antibody for 30 min at 4°C). Finally, cells were washed twice, stained with DAPI for 10 min at 4°C, washed twice with PBS and the single-cell suspensions transferred to 1.5 mL Eppendorf tubes for analysis by Amnis Imagestream (RRID:SCR_018589). For co-localisation with the lysosomes, Mϕ were pre-treated with Lysobrite Red (AAT Bioquest, 22645) following the manufacturer's protocol. Acquisition settings: Illumination intensity: 405 (20 mW), 488 (100 mW), 561 (50 mW), 642 (50 mW); Magnification: 40X; Speed: low. Cells were gated on the Scatter plot of Area vs Aspect Ratio of Brightfield. Live cells were gated on Scatter plots of channel 7 relative to DAPI.

RNA Isolation and Quantitative Real-Time PCR. Total RNA was extracted from treated cell lysates using the Allprep DNA/RNA/Protein Mini Kit (Qiagen; Cat# 80004) according to the manufacturer's instructions. RNA concentration and purity (A260/A280 and A260/A230 ratios) were assessed using a NanoDrop™ Spectrophotometer (Thermo Fisher Scientific). Equivalent amounts of high-quality total RNA (1μg/sample) were reverse-transcribed into complementary DNA (cDNA) using the High-Capacity cDNA Synthesis Kit (Bio-Rad; Cat# 1708891) under the following thermal cycling conditions: 25°C for 5 minutes, 46°C for 20 min, and 95°C for 1 min. Quantitative real-time PCR was performed using SsoFast Eva Green Supermix (BioRad, Cat# 172-5201). The reaction mixture contained 2 μL of diluted cDNA, 10 μL of Master Mix, and 2 μL of forward and reverse primers (100 μM) and nuclease-free water in a total volume of 20 μL. The specific primer sequences used for human targets were as follows: PD-L1 (CD274): Forward 5'- TGG CAT TTG CTG

Downloaded from aacrjournals.org/cancerres/article-pdf/doi/10.1158/0008-5472.CAN-25-5578/3827263/can-25-5578.pdf by University of Washington user on 07 September 2026

AAC GCA TTT-3'; Reverse 5'- TGC AGC CAG GTC TAA TTG TTT T-3'; Housekeeping Control (GAPDH): Forward 5'CTC CTC CAC CTT TGA CGC TG-3'; Reverse 5'-CAT ACC AGG AAA TGA GCT TGA CAA-3'. Thermocycling conditions (Bio-Rad CFX96) consisted of an initial denaturation at 95°C for 30 seconds, followed by 40 cycles of 95°C for 5 seconds and 58°C for 5 seconds. For SYBR Green assays, a melt curve analysis was performed immediately following amplification to verify primer specificity and the absence of primer-dimers. All samples were run in technical triplicates. Relative mRNA expression levels were calculated using the comparative threshold method (single Threshold). The expression of the target gene (CD274) was normalized to the endogenous reference gene (GAPDH) to calculate the δCt, and fold changes were determined relative to the media-treated control condition.

Western Blot analysis. 1x10^6 THP-1 cells were plated 24h before the experiment. Cells were incubated with complete growth medium supplemented with IFNγ (20 ng/ml). On the day of the experiment, cell media were replaced with serum-free media containing the PSE, $_{dn}$PDL1, or PBS and incubated for 0, 4, 16, 24, 48 hours. At the end of the assay, the supernatant was removed and the cells were lysed using RIPA cell lysis buffer supplemented with protease inhibitors cocktail and phosphatase inhibitors on ice for 30 min. The cells were centrifuged at full speed (13,000 rpm) for 15 min at 4°C. The supernatant was collected, and the protein concentrations were quantified using the BCA assay. The supernatants for each condition were split into equal amounts and supplemented with Laemmli buffer (4x). An equal amount of protein (about 30 μg, determined by BCA assay) was loaded per lane and separated on SDS-PAGE gels (SurePage Bis-Tris, 4-20%, 15-well, Tris-MOPS- SDS running buffer), and then transferred onto nitrocellulose membrane (BioRad TransBlot Turbo Transfer pack). Membranes were blocked for 1h with 5% non-fat dry milk in TBS supplemented with 0.05% Tween-20 (TBST) at room temperature for 1h and then probed with the primary antibody (anti-PD-L1, Cell Signaling Technology, N.13684, RRID:AB_2687655 or anti-Actinβ, BD Biosciences, N. 612657, RRID:AB_399901, 1:1,000 in blocking buffer) at 4°C overnight. After three times washing with TBST, secondary antibody (anti-goat, RRID: AB_2307391, or anti-rabbit, RRID: AB_2307391, IgG HRP-conjugated, 1:15,000 dilution in blocking buffer) is added to the membrane for 1h at room temperature. All membranes were washed three times

Downloaded from aacrjournals.org/cancerres/article-pdf/doi/10.1158/0008-5472.CAN-25-5578/3827263/can-25-5578.pdf by University of Washington user on 07 September 2026

and exposed using ECL substrate (West) and imaged at the Fusion X Vilber (RRID:023580).

Zebrafish Studies

Zebrafish Husbandry and Transgenic Lines. *Danio rerio* (zebrafish) models were maintained in accordance with the Champalimaud Fish Platform protocols and standard European Animal Welfare Legislation (Directive 2010/63/EU). All experimental protocols received ethical approval from the Champalimaud Animal Ethical Committee and Portuguese regulatory organizations, specifically ORBEA and DGAV. Depending on the specific experimental aims, double transgenic zebrafish models were utilized, which included the lines Tg(fli1:eGFP), Tg(mpeg1:mcherry-F), and Tg(mpeg1:mcherryF, tnfa:eGFP-F).

Cell Culture Conditions. The triple-negative breast cancer (TNBC) cell line Hs578T (RRID:CVCL_0332) was cultured in High Glucose DMEM (Biowest). The basal medium was supplemented with 10% fetal bovine serum (Sigma-Aldrich), 1% penicillin/streptomycin (10,000 U/mL, Hyclone), and 10 g/mL insulin (Sigma-Aldrich). The cells were maintained in a humidified incubator at 37°C with an atmosphere of 5% CO2. Cell line authenticity was confirmed via short tandem repeat (STR) profile analysis, and cultures were routinely screened to ensure they remained free of mycoplasma contamination.

Cell Labelling and Preparation. Once the Hs578T cells reached 70% confluence, they were washed with 1X Dulbecco's phosphate-buffered saline (DPBS, Biowest) and detached by scraping in 1 mM EDTA. The collected cell suspension was transferred into a 1.5 mL Eppendorf tube for staining. Cells were labeled with the lipophilic dye Deep Red Cell Tracker (Life Technologies) using 1 μL/mL of the dye in 1X DPBS (diluted from a 10 mM stock). The staining mixture was incubated in the dark for 10 minutes at 37°C. After incubation, the cells were washed with DPBS to remove excess dye and centrifuged at 250 × g for 4 minutes at 4°C. The resulting cell pellet was resuspended in DMEM. Cell viability was confirmed using the trypan blue exclusion method, and total cell counts were measured using a hemocytometer. Following quantification, the cells were resuspended in standard growth medium to achieve a precise final concentration of 0.5 × 10^6 cells/μL.

Downloaded from aacrjournals.org/cancerres/article-pdf/doi/10.1158/0008-5472.CAN-25-5578/3827263/can-25-5578.pdf by University of Washington user on 07 September 2026

Zebrafish Xenograft Injection and Treatment. Fluorescently labelled Hs578T cells were microinjected into the perivitelline space of 2 days post-fertilization zebrafish embryos (anesthetized with 1X Tricaine, Sigma-Aldrich) using borosilicate glass microcapillaries, a Zeiss Axio Zoom V16 microscope, and a PV820 Pneumatic Pico pump (World Precision Instruments). After a 10-minute recovery in 1X Tricaine, xenografts were maintained in E3 medium at 34°C. At 1 day post-injection, embryos with off-target cells or debris were discarded. Successful xenografts were size-matched (relative to eye size) and treated with E3 medium (control), ^{dn}PDL1, or ^{long}PSE, with all media and compounds refreshed daily. At 1 or 4 days post-injection, xenografts were sacrificed, fixed overnight at 4°C in 4% (v/v) formaldehyde (Thermo Fisher Scientific), and preserved in 100% (v/v) methanol at –20°C. To optimally preserve fluorescence, the Tg(mpeg1:mcherry-F) transgenic line was exclusively fixed using PIPES buffer rather than formaldehyde.

Confocal imaging and analysis of zebrafish xenografts. Mounted xenografts were imaged with an Andor BC43 spinning disk confocal microscope (20× objective, 5 μm z-stack intervals). Cells were manually counted using the ImageJ/Fiji Cell Counter plugin. Tumor size, utilized as a proxy for total DAPI nuclei, was estimated from three representative slices (top/Zfirst, middle/Zmiddle, bottom/Zlast) per z-stack using the following formula:

$$tumour\ size = \left(\frac{Zfirst + Zmiddle + Zlast}{3} \times total\ number\ of\ slices\right)/1.5$$

The 1.5 correction factor accounts for human nuclei averaging 10-12 μm in diameter. Additionally, TNFα-positive and negative macrophages were quantified across every slice and expressed as a percentage relative to the calculated tumor size.

Statistical analysis was performed using the GraphPad Prism 10.0 software. Data normality was assessed via D'Agostino-Pearson and Shapiro-Wilk tests. Normal datasets were evaluated using an unpaired parametric t-test, whereas non-normal datasets were analyzed with a nonparametric unpaired Mann–Whitney test. Fisher's exact test was exclusively applied to clearance datasets. All tests were two-sided with a confidence interval of 95%. Statistical significance was defined as *p<0.05, **p<0.01, ***p<0.001, ****p<0.0001. The bars indicate the results as AVG ± standard deviation of the mean (STDEV).

Downloaded from aacrjournals.org/cancerres/article-pdf/doi/10.1158/0008-5472.CAN-25-5578/3827263/can-25-5578.pdf by University of Washington user on 07 September 2026

Mouse Studies

Cell culture for the MC-38 murine model. C57BL/6 murine colon adenocarcinoma cell line MC-38 was purchased from Kerafast (ENH204-FP). The cell was cultured in DMEM (Gibco) with 10% FBS (Gibco, Thermo Fisher Scientific), 1x GlutaMAX (Gibco, Thermo Fisher Scientific), and 1x penicillin/streptomycin solution (Gibco, Thermo Fisher Scientific). The cell was cultured at 37ºC in humidified conditions with 5% CO2.

***In vivo* MC-38 colorectal cancer mouse studies**. All animal experiments were conducted at the Gulbenkian Institute for Molecular Medicine (GIMM, Lisbon). Animal work was performed in strict accordance with Portuguese Law (Portaria 1005/92) and the European Guideline 86/609/EEC, and followed the Federation of European Laboratory Animal Science Associations guidelines and recommendations concerning laboratory animal welfare. All animal experiments were approved by the Portuguese official veterinary department for welfare licensing – Direção Geral de Alimentação e Veterinária (DGAV) and the GIMM Animal Ethics Committee (authorization AWB_2021_03_GB_TargCancerDrugs).

Female C57BL/6J mice (8-10 weeks old; Charles River) were subcutaneously inoculated in the right flank with 1×10^6 MC-38 cells suspended in a 1:1 mixture of PBS and Matrigel (Corning). Tumor growth was monitored over time by performing bilateral vernier caliper measurements every day, and mean tumor volumes were calculated using the formula (length x width^2) /2. Treatments were initiated approximately 7-8 days post-induction once tumor volumes reached 90-100 mm³. For the initial efficacy study, MC-38 tumor-bearing mice were randomized to receive 10 mg/kg ^{long}PSE, 8.5 mg/kg $_{dn}$PDL1, 1 mg/kg Peptide, 50 μg/mouse Magrolimab, or Vehicle (PBS) as control. The doses of $_{dn}$PDL1 and Peptide were matched to the molar concentration of the ^{long}PSE group, while the Magrolimab dose was selected based on previously reported studies.[40] Treatments were administered intratumorally (i.t.) on days 7, 10, and 13 after tumor inoculation, with the mice being randomly assigned to receive ^{long}PSE, $_{dn}$PDL1, Magrolimab, Peptide, and PBS as controls. For the evaluation of next-generation half-life extended constructs, mice were randomly assigned to Vehicle (PBS), 1 mg/kg Peptide, 50 μg/mouse Magrolimab, 8.5 mg/kg $_{dn}$PDL1, 10 mg/kg ^{long}PSE, 12.8 mg/kg ABD-$_{dn}$PDL1, or 13.8 mg/kg ABD-^{long}PSE, and received three doses of i.t. injections on days 7, 10, and 13 (in all groups, the functional

Downloaded from aacrjournals.org/cancerres/article-pdf/doi/10.1158/0008-5472.CAN-25-5578/3827263/can-25-5578.pdf by University of Washington user on 07 September 2026

596 domains were used in equimolar amounts for direct, fair efficacy comparisons). To
597 assess pharmacological safety, animals were treated intravenously (i.v.) with a single
598 dose on day 7 of Vehicle (PBS), 1 mg/kg Peptide, 50 μg/mouse Magrolimab, 12.8
599 mg/kg ABD-$_{dn}$PDL1, or 13.8 mg/kg ABD-^{long}PSE. Body weight, tumor size, plasma AST
600 activity (day 0 and day 5), full blood counts, and histology of heart, lung, liver, kidney,
601 and spleen were evaluated at the indicated time points. Finally, in the repeated-dose
602 i.v. survival study, mice were randomized to Vehicle (PBS), 1 mg/kg Peptide, 12.8
603 mg/kg ABD-$_{dn}$PDL1, or 13.8 mg/kg ABD-^{long}PSE, and treated i.v. on days 7 and 10 (two
604 total doses). Animals were monitored daily for tumor growth and body weight. Mice
605 were euthanized if tumor volume reached 1,000 mm³, body weight loss exceeded
606 20%, or if tumors ulcerated. Housing consisted of individually ventilated cages with
607 HEPA-filtered air, maintaining a maximum of five mice per cage to minimize social
608 isolation. Environmental conditions were set to 20-24°C with 55 ± 10% relative
609 humidity and a 14h/10h light/dark cycle (lights on at 07:00). Autoclaved RM3A (P) diet
610 pellets (SDS Special Diets Services, 801030) and sterile reverse-osmosis water were
611 provided *ad libitum*. The data collected was analysed using GraphPad Prism v10.0.
612
613 **Haematotoxicity, liver function, and histopathology.** AST activity was determined
614 using an Aspartate Aminotransferase Activity Assay Kit (abcam, ab105135), and
615 complete blood counts [WBC (White Blood Cell Count), RBC (Red Blood Cell Count),
616 HGB (Haemoglobin), PLT (Platelet Count), HCT (Haematocrit), MCV (Mean
617 Corpuscular Volume), PDW (Platelet Distribution Volume), MPV (Mean Platelet
618 Volume)] were obtained using a PocH-100iV - Haematology Analyzer. For histological
619 evaluation, organs were harvested, fixed in 10% formalin, embedded in paraffin,
620 sectioned into 3 μm-thick sections, and stained with Haematoxylin and Eosin (H&E).
621 Whole sections were acquired with the NanoZoomer-SQ Digital slide scanner
622 (Hamamatsu), and pathology assessment was performed by an experimental
623 pathologist (PF) at GIMM's Histopathology Facility. Scale bars: 100 μm.
624
625 **Cell Culture for KPC cell.** Murine pancreatic ductal adenocarcinoma KPC cells
626 (RRID:CVCL_M532) were cultured in high glucose with pyruvate DMEM (Gibco,
627 Thermo Scientific) supplemented with 10% v/v FBS (Gibco, Thermo Scientific) and 1%

Downloaded from aacrjournals.org/cancerres/article-pdf/doi/10.1158/0008-5472.CAN-25-5578/3827263/can-25-5578.pdf by University of Washington user on 07 September 2026

v/v P/S (Gibco, Thermo Scientific). Cells were maintained at 37°C in a humidified incubator equilibrated with 5% CO_2.

Animals. Female C57BL/6J mice (7-8 weeks old) were purchased from Charles River (RRID:IMSR_JAX:000664) and housed in the animal facility of the Faculty of Pharmacy at the University of Lisbon. All procedures were conducted in compliance with the Faculty of Pharmacy, University of Lisbon guidelines and approved by the Portuguese competent authority for animal protection, Direção-Geral de Alimentação e Veterinária (Reference 0421/000/000/2021). Mice were housed under a 12h light/12h dark cycle with food and water provided ad libitum, and all handling complied with NIH and European Union guidelines for laboratory animal care (Directive 2010/63/EU). Body weight was monitored three times per week. Animals were euthanized according to ethical protocol when showing signs of distress or with rapid weight loss (above 10% within a few days or 20% from the initial weight).

***In vivo* KPC mouse study.** On day 0, female C57BL/6J mice were orthotopically inoculated in the pancreas. Prior to inoculation, animals were anesthetized with ketamine and xylazine according to body weight (100 μL/10 g), a ~1 cm longitudinal incision was made on the left flank, at the level of the spleen projection. Carefully, the pancreas was pulled out of the incision and injected with 40 μL of a cell suspension containing 2.5×10^5 KPC cells (mycoplasma-free) in PBS mixed 1:1 with growth factor–reduced Matrigel (Corning). After tumor injection, the organs were carefully repositioned, and the peritoneum and skin were sutured. Analgesia (buprenorphine hydrochloride, Bupaq) was administered subcutaneously according to body weight. Mice were placed on a heated pad until fully awake and active. On day 5 after tumor inoculation, animals were randomized into different groups (N = 10): Vehicle (PBS), Magrolimab (50 μg/mouse), ABD-$_{dn}$PDL1 (12.8 mg/kg), Peptide (1.0 mg/kg), and ABD-^{long}PSE (13.8 mg/kg). Treatments were administered via intravenous (tail vein) injection. On day 15, four mice per group were sacrificed for tumor and spleen collection to analyse tumor-infiltrating and systemic immune cell populations. The remaining animals were monitored for survival. Mice were euthanized upon exhibiting signs of distress or significant weight loss as described above.

Downloaded from aacrjournals.org/cancerres/article-pdf/doi/10.1158/0008-5472.CAN-25-5578/3827263/can-25-5578.pdf by University of Washington user on 07 September 2026

Characterization of Tumor-Infiltrating Immune Populations and Spleen Immune Populations. Tumors and spleens were isolated from four animals per group, directly after euthanasia and systemic PBS perfusion, and placed in cold sterile PBS (pH 7.4). Tumor single-cell suspensions were obtained by mechanical dissociation followed by enzymatic digestion for 30 min at 37°C. Enzymatic digestion solution was prepared in HBSS (Gibco, Thermo Scientific) with 2 mg/mL collagenase type II (Worthington Biochemical Corporation) and DNAse (Worthington Biochemical Corporation). The digested suspension was filtered through a 70 μm cell strainer, centrifuged at 300 x *g* for 5 min at 4°C, and resuspended in cold PBS (pH 7.4). Spleens were mechanically dissociated, and erythrocytes were lysed using ACK buffer for 5 min at 37°C. The resulting suspension was filtered through a 70 μm strainer, centrifuged at 300 x *g*, 5 min, 4°C, and resuspended in cold PBS (pH 7.4).

For both tissues, cells were seeded into 96-well plates (5×10^6 cells/well). Live/dead discrimination was performed using Ghost Dye® Red 780 (Cytek) (1:5,000). Fc receptors were blocked with TruStain FcX™ PLUS CD16/32 (BioLegend) for 10 min at room temperature. Surface staining was performed with fluorochrome-labeled anti-mouse antibodies, followed by fixation and permeabilization using the eBioscience Foxp3/Transcription Factor Staining Buffer Set (Thermo Scientific). Intracellular staining was then conducted according to the manufacturer's instructions. The samples were acquired using the Cytek Aurora flow cytometer (Cytek). Data were analysed using FCS Express (De Novo Software).

Antibody panels for flow cytometry. For the analysis of T, B, and NK cells, the following panel of anti-mouse antibodies was used: anti-CD45 (RY703, clone 30-F11, 1:150, RRID: AB_3686544); anti-CD3 (RB744, clone 17A2, 1:160, RRID: AB_3685764); anti-CD4 (PerCP-Cy5.5, clone GK1.5, 1:80, RRID: AB_3685412); anti-CD8 (AF700, clone 53-6.7, 1:50, RRID: AB_493702); anti-CD19 (BV650, clone 6D5, 1:50, RRID: AB_11204087); anti-B220 (APC-Fire 810, clone RA3-6B2, 1:300, RRID: AB_2860603); anti-CD25 (PE-Cy5, clone PC61, 1:80, RRID: AB_312859); anti-CD44 (Pe-Cy7, clone IM7, 1:80, RRID: AB_830786); anti-CD107b (AF647, clone M3/84, 1:200, RRID: AB_493311); anti-PD-1 (PE, clone 29F.1A12, 1:50, RRID: AB_1877121); anti-MHCII (BV510, clone M5/114.15.2, 1:30, RRID: AB_2741133); anti-NK1.1 (BV570, clone PK136, 1:40, RRID: AB_2563286); and anti-FoxP3 (eFluor450, clone FJK-16s, 1:333, RRID: AB_1518812).

Downloaded from aacrjournals.org/cancerres/article-pdf/doi/10.1158/0008-5472.CAN-25-5578/3827263/can-25-5578.pdf by University of Washington user on 07 September 2026

For the analysis of myeloid cells, the following panel of anti-mouse antibodies was used: anti-CD45 (RY703, clone 30-F11, 1:150, RRID: AB_3686544); anti-CD11b (BV785, clone M1/70, 1:80, RRID: AB_2561373); anti-CD11c (PE-Cy5, clone N418, 1:80, RRID: AB_493566); anti-CD103 (BV605, clone 2E7, 1:30, RRID: AB_2872685); anti-CD80 (RB705, clone 16-10A1, 1:80, RRID: AB_3685835); anti-CD86 (AF700, clone GL-1, 1:80, RRID: AB_493720); anti-F4/80 (BV650, clone BM8, 1:40, RRID: AB_2564589); anti-PD-L1 (APC/Cy7, clone 10F.9G2, 1:50, RRID: AB_10612935); anti-CD206 (BV711, clone C086C2, 1:40, RRID: AB_2565822); anti-CD31 (PE-eFluor610, clone 390, 1:158, RRID: AB_312902); anti-Ly6C (PE, clone HK1.4, 1:300, RRID: AB_1186133); anti-Ly6G (APC, clone 1A8, 1:300, RRID: AB_1877163); and anti-MHCII (BV510, clone M5/114.15.2, 1:30, RRID: AB_2561397). See Supplementary Tables S3 and S4.

Sample size determination. Sample size was determined according to the prior work executed in the laboratory or from published reports of similar scope within the appropriate fields.[41]

Statistical Analysis. Statistical analyses were performed using GraphPad Prism software (v10; GraphPad Software; RRID: SCR 002798). Data are presented as mean ± standard error of the mean (SEM) or standard deviation (SD) as indicated. Comparisons between two groups were performed using a two-tailed Student's *t*-test. Multiple group comparisons were analyzed using ANOVA followed by Tukey's or Sidak's post-hoc tests. Survival data were analyzed using the Kaplan-Meier method, and differences evaluated using the log-rank test. A p-value of < 0.05 was considered statistically significant.

Replication. The number of biological replicates (typically $n \geq 3$) is indicated in the figure legends. Key findings were replicated in at least two independent experiments.

Data availability. Raw data are available upon request. Correspondence and requests for materials should be addressed to V.S. valerio.sabatino@unibas.ch, and/or G.J.L.B. gb453@cam.ac.uk.

Downloaded from aacrjournals.org/cancerres/article-pdf/doi/10.1158/0008-5472.CAN-25-5578/3827263/can-25-5578.pdf by University of Washington user on 07 September 2026

RESULTS

Phagocytic synapse enhancers (PSEs) are modular, bifunctional molecules designed to target the tumor microenvironment. To engage macrophages in proximity of cancer cells, the bifunctional PSE construct uses maleimide chemistry and a PEG linker to connect a *de novo* PD-L1 binder[38] ($_{dn}$PDL1) to tuftsin (Thr-Lys-Pro-Arg, TKPR), an IgG-derived immunomodulatory peptide that enhances phagocytosis (**Fig. 1a, b**).[42-51]

Tuftsin was conjugated to an $_{n}$PEG$_3$-maleimide linker (n=1 or 3) via its lysine ε-amino group, yielding two bifunctional molecules: ^{short}PSE and ^{long}PSE (**Fig. 1c-d**). Both constructs were characterized by mass spectrometry, while Octet biolayer interferometry (BLI) confirmed high-affinity PD-L1 binding (**Fig. 1c-d**) by retaining low-nanomolar affinity (^{short}PSE: K_D = 5.7 nM, ^{long}PSE: K_D = 5.8 nM). To confirm PSE binding to PD-L1$^+$ cells, we developed a fluorescent probe ^{FITC}PSE that successfully stained IFNγ-stimulated MC-38 cells overexpressing PD-L1 (**Fig. 1e-f**), with target engagement further validated through microscopy (**Supplementary Fig. 1a**) and competitive assays showing that the PSE blocks anti-PD-L1-APC staining in various tumor lines (**Supplementary Fig. 1b-c**).

PSEs bind macrophages through the tuftsin binding partner, neuropilin-1, and induce a pro-inflammatory response

We evaluated tuftsin's Mϕ-stimulating activity by treatment with NeutrAvidin Oregon Green 488 (NOG_{488}) complexed with biotinylated TKPR, which resulted in increased fluorescence uptake in RAW 264.7 Mϕ (**Fig. 2a-c**). The uptake is suppressed when the tuftsin antagonist (TKPPR) is present, confirming the tuftsin-mediated uptake (**Supplementary Fig. S2a-c**)**.** To validate the activity of tuftsin in the context of the PSEs, we assessed the binding to its previously reported putative receptors, neuropilin-1 (NRP1) and FcRs.[45,47,48,50] BLI analysis (**Fig.2d-f**) showed similar NRP1 binding kinetics for the peptide and ^{long}PSE (K_D ^{long}PSE= 72 nM; K_D Peptide= 102 nM), while unconjugated $_{dn}$PDL1 did not bind NRP1. Therefore, tuftsin acts through NRP1 both as a free peptide and as a conjugate. We then assessed FcγRs binding by surface plasmon resonance (SPR) analysis against FcγRIa, FcγRIIa, FcγRIIb, and FcγRIIIa (**Supplementary Fig. S2d**). Both $_{dn}$PDL1 and ^{long}PSE displayed unspecific binding with the antibody used to immobilize the FcγRs. However, and more importantly, the

Downloaded from aacrjournals.org/cancerres/article-pdf/doi/10.1158/0008-5472.CAN-25-5578/3827263/can-25-5578.pdf by University of Washington user on 07 September 2026

peptide alone did not bind any of the FcγRs, excluding any FcγR-mediated activity of tuftsin.

To evaluate the effect of the PSE on macrophages, the expression of classical polarization surface markers was analyzed across four independent biological donors (n=4) and normalized to a baseline control (**Fig. 2g-h**). At 24 hours treatment, the Mϕ shift toward a pro-inflammatory state, with an increase in CD86 and MHC-II and a robust upregulation of PD-L1. Concurrently, the treatment induced a consistent suppression of classical anti-inflammatory markers, CD163 and CD206, and downregulation of NRP1. Quantification of the culture supernatant (**Fig. 2i**) confirmed that the treatment induces a robust pro-inflammatory secretome, characterized by upregulated cytokines (TNFα, IL-6, and IL-8) and chemokines (CCL2, CCL3, CCL5, CXCL1, CXCL10), alongside downregulated IL-1ra. We confirmed these findings *in vivo* using a double-transgenic zebrafish xenograft model Tg(mpeg1:mCherry-F; tnfa:eGFP-F)[52-54], where TNFα secretion distinguishes Mϕ populations (M_1-like/pro-inflammatory = mpeg$^+$/tnf$^+$; M_2-like/anti-inflammatory = mpeg$^+$/tnf$^-$, (**Supplementary Fig. S3a**). Treatment with ^{long}PSE and Peptide increased the abundance of pro-inflammatory Mϕ while treatment with the unconjugated binder ($_{dn}$PDL1) was comparable to control (mpeg$^+$/tnf$^+$, **Supplementary Fig. S3b-c**). As zebrafish embryos at 2 days post-fertilization lack a mature adaptive immunity, the observed effects can be entirely attributed to innate immune modulation. Together, these results indicate that PSE treatment overrides baseline cellular suppression to establish a tuftsin-driven pro-inflammatory profile.

PSEs boost PD-L1 endocytosis and lysosomal trafficking in PD-L1$^+$ macrophages

Previous studies have shown that PD-L1 is broadly expressed within the TME, not only by tumor cells, but also by immunosuppressive Mϕ.[55-58] We used PD-L1-expressing Mϕ to investigate the effect of the PSE when both targets are present on the same cell. Using ^{FITC}PSE, we tracked both PSE (by FITC staining) and PD-L1 (by anti-PDL1-APC staining) after 30-min and 4-hour incubations (**Fig. 3a-c**). After 4 hours, ^{FITC}PSE (green channel) internalised and co-localised with PD-L1 (red channel) in the lysosomes (yellow channel). Moreover, treatment with both $_{dn}$PDL1 and ^{long}PSE markedly reduced surface PD-L1 staining after 4 hours incubation due to competitive

Downloaded from aacrjournals.org/cancerres/article-pdf/doi/10.1158/0008-5472.CAN-25-5578/3827263/can-25-5578.pdf by University of Washington user on 07 September 2026

blockade/internalization of the target (**Fig. 3d**). Co-localization analysis further revealed that ^{long}PSE induced a 2-fold increase in PD-L1 lysosomal localization compared to $_{dn}$PDL1, whereas untreated controls (media only) showed no PD-L1 internalization, with staining restricted to the cell surface (**Fig. 3e-f**).

These results suggest that the PSE favors a 'cis-targeting' setup in PD-L1$^+$ Mϕ, which internalize and direct PD-L1 into the lysosomes.[59]

Tracking the his-tagged PSE revealed striking cell-specific differences in internalization dynamics: while PD-L1$^+$ Mϕ rapidly internalized >50% of PSE within 4 hours and subsequently lost surface PD-L1 (**Supplementary Fig. S4a-d**), tumor cells retained PSE almost entirely on their surface with minimal (~7%) internalization even after 24 hours (**Supplementary Fig. S4e-h**). This discrepancy, driven by the inherently higher membrane turnover of macrophages, results in two distinct modes of action within the tumor microenvironment: sustained surface blockade on cancer cells versus an internalizing "sink" activity in macrophages. Although this sink effect diverts PSE from direct tumor binding, it potentially enhances broader anti-tumor immunity by targeting immunosuppressive PD-L1$^+$ Mϕ and preventing PD-L1/CD80 cis-heterodimerization, freeing CD28 to effectively activate T cells.[60]

Analysis of the Mϕ lysates demonstrated a reduction of total PD-L1 following ^{long}PSE treatment over 48-hour (**Supplementary Fig. S4i**). Importantly, steady-state protein quantification underestimates absolute degradation due to PSE-driven upregulation (~2-fold vs control) of PD-L1 mRNA (**Supplementary Fig. S4j**). To prove that rapid lysosomal turnover was counteracting this transcriptional surge, we co-administered the lysosomal inhibitor chloroquine (CQ). Blocking the lysosomal activity unmasked this dynamic clearance, leading to a 74% increase of total PD-L1 in PSE-treated cells versus inhibitor-only control (**Supplementary Fig. S4k**). Overall, ^{long}PSE treatment increases PD-L1 lysosomal trafficking by more than 7-fold compared to basal turnover. These findings validate that the PSE accelerates PD-L1 turnover in PD-L1$^+$ Mϕ and directs surface PD-L1 into the lysosomal compartment.

PSEs promote the endocytosis of soluble extracellular targets in macrophages

We sought to verify whether the PSE also promotes the internalization of soluble extracellular PD-L1 via tuftsin-dependent mechanism in macrophages with low or

Downloaded from aacrjournals.org/cancerres/article-pdf/doi/10.1158/0008-5472.CAN-25-5578/3827263/can-25-5578.pdf by University of Washington user on 07 September 2026

absent PD-L1 expression. We used a biotinylated PD-L1 (Biot-PDL1) complexed to NOG_{488} to generate NOG-PDL1 fluorescent complex, which was incubated with ^{long}PSE or controls in the presence of non-polarized Mϕ (**Fig. 3g**). ^{long}PSE induced strong internalization of NOG-PDL1, attributable to the tuftsin-mediated endocytosis (**Fig. 3h-i**). This approach was further extended to target EGFR, using a de novo EGFR binder ($_{dn}$EGFR) to assemble EGFR-targeting PSEs (**Supplementary Fig. S5a-d**). Similarly, incubation of EGFR-^{long}PSE with Mϕ resulted in the internalization of the NOG-EGFR complex (**Supplementary Fig. S5e-f**). Because these findings suggest that Mϕ internalize PSE-targeted antigens via a tuftsin-dependent mechanism even without the target antigen present on their membrane, we envision this approach can be further tuned to direct proteins of interest to specific macrophage compartments, such as lysosomes, dedicated to protein degradation.[61-66]

The intercellular activity of the PSEs increases the avidity between macrophages and tumor cells, thereby enhancing phagocytosis.

Having established the effects of PSEs in monocultures, we transitioned to co-culture systems to determine whether the bifunctional molecules could bridge Mϕ and cancer cells, thereby promoting the cell-to-cell proximity needed to initiate phagocytosis. For this purpose, we synthesized an expanded PSE library for screening activity (**Supplementary Fig. S6**). First, we used acoustic force spectroscopy to measure intercellular avidity in a co-culture of PD-L1-overexpressing MC-38 tumor cells and non-polarized, PD-L1-deficient Mϕ, a setup designed to favor PSE trans-targeting (**Fig. 4a**). After optimizing the concentration range, we observed that binding strength increased from 12.5 nM to 1.25 μM but dropped at 12.5 μM, indicating a classic Hook effect[67] (**Supplementary Fig. S6d**). We therefore performed avidity experiments at 125 nM. Both ^{short}PSE and ^{long}PSE induced higher avidity than the peptide alone (**Fig. 4a, Supplementary Fig. S6e**), indicating that antigen binding is essential for strengthening effector–target interactions. This study establishes a first methodology for quantifying avidity using Mϕ as effector cells, providing a framework for future optimization and systematic screening of Mϕ–engaging molecules.

The observed increase in avidity directly correlated with enhanced phagocytosis. Both confocal microscopy and flow cytometry confirmed that ^{long}PSE induced a more than 2-fold increase in phagocytic activity compared to media controls (**Fig. 4b-d**).

Downloaded from aacrjournals.org/cancerres/article-pdf/doi/10.1158/0008-5472.CAN-25-5578/3827263/can-25-5578.pdf by University of Washington user on 07 September 2026

Increasing the concentration from 100 nM to 1 μM did not further enhance phagocytosis (**Fig. 4e**), while the phagocytic efficacy of ^{long}PSE was comparable to Magrolimab® (**Fig. 4f**).

Screening activity of the PSE library (**Supplementary Fig. S6a-c**) revealed that ^{long}PSE consistently yielded the highest phagocytic index (**Supplementary Fig. S6f-g**). Notably, the enhanced effect was abolished when tumor cells were not pre-treated with IFNγ (**Supplementary Fig. S6h**), confirming that PD-L1 expression is essential for establishing the phagocytic synapse.

We validated the PD-L1-dependent PSE activity using GL-261 tumor cells and its engineered PD-L1 knockout variant, GL-261 PDL1^{KO} (**Supplementary Fig. S6i-j**). In GL-261 cells, ^{long}PSE enhanced phagocytosis (**Supplementary Fig. S6i**), whereas no differences were observed among treatments in GL-261 PDL1^{KO} cells, apart from an elevated basal phagocytic rate in the absence of PD-L1 (**Supplementary Fig. S6j**).

To assess whether macrophage polarization influences PSE efficacy, THP-1 Mϕ were pre-treated with IFNγ/LPS or IL-4 (**Supplementary Fig. S6k-l**). In co-cultures with engineered U87 tumor cells expressing a blue fluorescent reporter (PB450^{+} cells), ^{long}PSE successfully drove phagocytosis regardless of baseline macrophage polarization, demonstrating significant efficacy in both pro-inflammatory and anti-inflammatory Mϕ states (**Supplementary Fig. S6k-l**). Collectively, these data demonstrate that PSEs enhance Mϕ-mediated phagocytosis across diverse co-culture systems. The efficacy of PSEs depends on target expression, yet the enhancement of phagocytosis occurs independently of macrophage polarization state. Therefore, even when PD-L1 is targeted on both tumor cells and Mϕ, the phagocytic activity is enhanced.

In vivo PSE treatment in a syngeneic colorectal carcinoma improves survival with modest effect

We used ^{long}PSE in efficacy studies with a syngeneic mouse model of colorectal carcinoma (CRC) (**Fig. 4g**). Most solid tumors overexpress immune checkpoints such as PD-L1 (“don’t find me”) and CD47 (“don’t eat me”) to evade immune detection,[68] and the MC-38 subcutaneous model is well established for investigating these immune checkpoints.[69,70] The TME of the engrafted mice upregulates PD-L1 on both tumor cells and myeloid cells, anticipating a more favorable outcome when the PSE targets

Downloaded from aacrjournals.org/cancerres/article-pdf/doi/10.1158/0008-5472.CAN-25-5578/3827263/can-25-5578.pdf by University of Washington user on 07 September 2026

both populations.[60,71] We treated the mice intratumorally (i.t.) and daily monitored their body weight and tumor size (**Fig. 4h-i**). The ^{long}PSE treatment delayed tumor progression and extended overall survival, although the improvement was modest relative to Magrolimab® or tuftsin peptide alone (**Fig. 4j)**. The short half-life of $_{dn}$PDL1 ($t_{1/2}$ ≈ 15 min) likely limits PSE efficacy, suggesting that extending binder half-life in circulation could improve therapeutic outcomes.

Next-generation PSEs with extended half-life lead to a greater improvement of *in vivo* efficacy.

To overcome this limitation, we developed an improved binder, ABD-$_{dn}$PDL1, by fusing $_{dn}$PDL1 to an albumin-binding domain (ABD) to extend PSE's half-life ($t_{1/2}$ ~12 h, **Fig. 5a**).[72] The resulting bifunctional ABD-^{long}PSE (~20 kDa) retained PD-L1 binding activity equivalent to ^{long}PSE and the unconjugated binder (**Fig. 5b-c**). The fusion constructs were tested in co-culture with engineered Jurkat T cells expressing PD-1 together with a luciferase reporter driven by NFAT, and CHO-K1 target cells expressing PD-L1 and a TCR activator (**Fig. 5d**). Atezolizumab was used as positive control to follow PD-1/PD-L1 blockade by bioluminescence analysis (**Fig. 5e**). Both engineered constructs ABD-$_{dn}$PDL1 and ABD-^{long}PSE efficiently inhibited PD-1/PD-L1 signaling, reaching full blockade at 30 nM (EC_{50}= 3nM).

In a syngeneic CRC model, i.t. administration of ABD-^{long}PSE markedly improved survival compared to all other groups, including the phagocytosis enhancer Magrolimab (**Fig. 5f**). The extended-half-life binder (ABD-$_{dn}$PDL1) also outperformed $_{dn}$PDL1 and exhibited comparable efficacy to ^{long}PSE, confirming that half-life extension boosts tumor control. Subsequent experiments using intravenous (i.v.) administration confirmed that ABD-^{long}PSE achieves superior tumor control with a single injection compared to all other conditions (**Supplementary Fig. S7a)**. The treatment was well-tolerated, with no indications of hepatic damage or broader systemic toxicity observed upon histo/haematological evaluation (**Supplementary Fig. S7b-d**). Repeated dosing on days 7 and 10 further delayed tumor growth and extended survival (**Fig. 5g**), highlighting the superior efficacy of ABD-^{long}PSE across different administration routes.

PSE treatment improves survival and modulates immunity in an orthotopic pancreatic cancer model.

Downloaded from aacrjournals.org/cancerres/article-pdf/doi/10.1158/0008-5472.CAN-25-5578/3827263/can-25-5578.pdf by University of Washington user on 07 September 2026

We tested the translational potential of ABD-^{long}PSE in an aggressive model of pancreatic cancer characterized by a dense stroma that prevents effective drug delivery and immune cell infiltration. Pancreatic cancer often shows poor antigenicity and is dominated by immunosuppressive cells, such as myeloid-derived suppressor cells (MDSCs) and regulatory T cells (T_{regs}), which neutralize anti-tumor immunity.[73-75] KPC tumors (Kras^LSL-G12D/+; Trp53^LSL-R172H/+; Pdx1-Cre)[73] were implanted orthotopically and treated i.v. (**Fig. 6a-b**). ABD-^{long}PSE significantly reduced tumor burden and prolonged survival, while Magrolimab®, ABD-$_{dn}$PDL1, and the peptide alone showed modest effects (**Fig. 6b**).

Flow cytometric analysis revealed immune modulation within the TME (**Fig. 6c-d**). All treatment groups increased CD45$^+$ infiltration versus vehicle (**Fig. 6c**). ABD-^{long}PSE treatment reduced total T cells, particularly T_{regs}, while NK cells increased (**Fig. 6c**, panels *i-iv*). Interestingly, CD4$^+$ and CD8$^+$ T cells in ABD-^{long}PSE-treated tumors expressed lower PD-1 levels than those in the ABD-$_{dn}$PDL1 group (**Fig. 6c**, panels *vii-viii*). ABD-^{long}PSE treatment drove profound changes in the myeloid compartment, specifically reducing the frequency of MDSCs and TAMs over 2-fold compared to vehicle (**Fig. 6d,** panels *i-v*). Furthermore, the remaining TAMs undergo phenotypic shift as they display higher CD80 and lower CD206 compared to vehicle (**Fig. 6d,** panels *vi-viii*). Interestingly, ABD-$_{dn}$PDL1 treatment increased PD-L1 expression on TAMs and dendritic cells, whereas ABD-^{long}PSE prevented this upregulation, suggesting tuftsin conjugation mitigates compensatory immunosuppression. Together, these results demonstrate that ABD-^{long}PSE effectively modulates both myeloid and lymphoid compartments, leading to improved tumor control and survival in a more aggressive cancer model.

Discussion

To overcome the challenges of tumor heterogeneity and complex immune-tumor interactions, we developed a strategy that combines PD-L1 blockade with innate immune engagement. While conceptually related to bispecific macrophage engagers (BiMEs), our PSEs *i)* do not engage myeloid cells via FcRs, *ii)* are small enough (~15-20 kDa) to penetrate the dense stroma, *iii)* display a natural “eat me” signal, and *iv)*

Downloaded from aacrjournals.org/cancerres/article-pdf/doi/10.1158/0008-5472.CAN-25-5578/3827263/can-25-5578.pdf by University of Washington user on 07 September 2026

actively clear immunosuppressive checkpoints by driving cis-targeted PD-L1 endocytosis in macrophages.

The therapeutic efficacy of the PSE platform relies on the balance of target antigens and effector cells within the TME. Tumors characterized by high PD-L1 expression and dense myeloid infiltration are optimal candidates for this approach. Moreover, the PSEs can potentially prime "cold," immune-excluded tumors that historically resist PD-L1 blockade. Because PSE treatment initiates a localized pro-inflammatory cytokine cascade that boosts target expression, the therapy can remodel the suppressive architecture of the TME even when tumor-intrinsic PD-L1 expression is modest.

Our study highlights the translational potential of the PSEs, demonstrated by profound *in vivo* TME remodeling, though key steps remain for clinical development. First, current efficacy relies on PD-L1 expression, although the platform's modularity allows it to be adapted for PD-L1-negative tumors. Second, the exact interplay between innate and adaptive immune responses must be further decoupled. Most crucially, while murine models showed no acute toxicity, the intentional induction of a robust pro-inflammatory secretome (IL-6, IL-8, TNFα) raises the risk of "on-target, off-tumor" cytokine release syndrome. Advancing this therapy to the clinic requires comprehensive pharmacokinetic, biodistribution, and toxicology studies in higher-order species to define a safe therapeutic index and ensure immune activation remains localized to the tumor.

This study represents a first step toward the therapeutic application of PSEs in cancer immunotherapy. The modular approach provides a versatile, highly tunable platform of immune engagers capable of targeting diverse tumor-associated antigens, ultimately reprogramming the TME and boosting anti-tumor immunity.

Acknowledgements

V. Sabatino acknowledges support from the Swiss National Science Foundation (P500PN_202711, P5R5PB_217904). C. Tang acknowledges Fundação para a Ciência e a Tecnologia Portugal (2022.08101.CEECIND). This work was further supported by a Swiss National Science Foundation Professorial Fellowship (PP00P3_176974) and Swiss Cancer Research grants to G. Hutter (KFS-4382-02-2018 and KFS 5789-02-2023), Bridge Discovery Grant (40B2-0_237764), and

Downloaded from aacrjournals.org/cancerres/article-pdf/doi/10.1158/0008-5472.CAN-25-5578/3827263/can-25-5578.pdf by University of Washington user on 07 September 2026

Novartis Foundation grant (24B120) to G. Hutter and V. Sabatino, Xi'an Fengcheng Hospital (to G.J.L. Bernardes), and the Wellcome Developing Concept Fund (to G.J.L.Bernardes and V. Sabatino). A.R. Coelho acknowledges Fundação para a Ciência e a Tecnologia, Portugal (2023.06183.CEECIND). This research was made possible with support from the Histopathology Facility at GIMM. H.F. Florindo thanks the UID 04138 - Instituto de Investigação do Medicamento project supported by The Fundação para a Ciência e Tecnologia-Ministério da Ciência, Tecnologia e Ensino Superior (FCT-MCTES); "la Caixa" Foundation under the framework of the Healthcare Research call 2024 (LCF/PR/HR24/00968, PINT). R.C. Acúrcio is supported by the FCT-MCTES (2023.08262.CEECIND/CP2843/CT0002).

Author Contributions

V. Sabatino and G.J.L. Bernardes conceived the study. V. Sabatino designed, synthesised and characterised the PSEs, designed and performed biological assays, visualised and analysed the data, wrote the manuscript. C. Tang, C. Labao-Almeida, A.R. Coelho. performed *in vivo* studies and analysis with CRC model. D. Hicks and W. Yang produced $_{dn}$PDL1, ABD-$_{dn}$PDL1 and $_{dn}$EGFR. F. Müller and W.T. Khaw synthesised PSEs in larger scale for the *in vivo* studies. I. Sarkar, D. Shome and R. Reimers designed, performed, and analyzed avidity assays with the support of V. Sabatino. A. Vasco synthesised the peptide cTKPRG. M. Cabeza-Cabrerizo. produced nbPD-L1 and helped with microscopy experiments. T. Rohm helped with the phagocytosis assays and flow cytometric analysis. F. Gerster performed PBMC isolation and primary monocyte extraction. S. Fleisch performed *in vitro* experiments with GL-261 cell lines. A. Gerber performed qPCR and gene expression analysis. D. Kaymak helped with flow cytometric analysis. M. Fontes and R. Fior designed and performed zebrafish experiments. R.C. Acúrcio and H.F. Florindo performed *in vivo* study and immune characterisation with the KPC model. S. Pantelyushin. and J. vom Berg generated the GL-261 PDL1^{KO} cell line. G. Hutter co-supervised and allocated resources. G.J.L. Bernardes coordinated and supervised the project, allocated resources, and co-wrote the manuscript. The manuscript was finalised with contributions from all authors

Downloaded from aacrjournals.org/cancerres/article-pdf/doi/10.1158/0008-5472.CAN-25-5578/3827263/can-25-5578.pdf by University of Washington user on 07 September 2026

References

1. Topalian, S.L., Sharpe, A.H. Balance and imbalance in the immune system: life on the edge. *Immunity* **41**, 682-684 (2014).
2. Postow, M.A., Callahan, M.K., Wolchok, J.D. Immune Checkpoint Blockade in Cancer Therapy. *J. Clin. Oncol.* **33**, 1974-1982 (2015).
3. Kubli, S.P., Berger, T., Araujo, D.V., Siu, L.L., Mak, T.K. Beyond immune checkpoint blockade: emerging immunological strategies. *Nat. Rev. Drug. Discov.* **20**, 899-919 (2021).
4. Leach, D.R., Krummel, M.F., Allison, J.P. Enhancement of antitumor immunity by CTLA-4 blockade. *Science* **271**, 1734-1736 (1996).
5. Kalbasi, A., Ribas, A. Tumour-intrinsic resistance to immune checkpoint blockade. *Nat. Rev. Immunol.* **20**, 25-39 (2020).
6. Gordon, S. Phagocytosis: An Immunobiologic Process. *Immunity* **44**, 463-475 (2016).
7. Quail, D., Joyce, J. A. Microenvironmental regulation of tumor progression and metastasis. *Nat. Med.* **19**, 1423-37 (2013).
8. DeBerardinis, R. J. Tumor microenvironment, metabolism, and immunotherapy. *N. Engl. J. Med.* **382**, 869-871 (2020).
9. Kirchhammer, N., Trefny, M. P., Auf der Maur, P., Läubli, H., Zippelius, A. Combination cancer immunotherapies: Emerging treatment strategies adapted to the tumor microenvironment. *Sci. Trans. Med.* **14**, eabo3605 (2022).
10. Noy, R., Pollard, J. W. Tumor-Associated Macrophages: From Mechanisms to Therapy. *Immunity* **41**, 49-61 (2014).
11. Cassetta L, Pollard, J.W. Targeting macrophages: therapeutic approaches in cancer. *Nat. Rev. Drug. Discov* **12**, 887-904 (2018).
12. Pathria, P., Louis, T.L., Varner, J. A. Targeting tumor-associated macrophages in cancer. *Trends Immunol*. **40**, 310-327 (2019).
13. Rolin, C., Zimmer, J., Seguin-Devaux, C. Bridging the gap with multispecific immune cell engagers in cancer and infectious diseases. *Cell. Mol. Immunol.* **7**, 643-661. 2024.
14. Scott, E. M., Jacobus, E., Lyons, B., Frost, S., Freedman, J. D., Dyer, A., Khalique, H., Taverner, W. K., Carr, A., Champion, B. R., Fisher, K. D., Seymour, L. W., Duffy, M. R. Bi- and tri-valent T cell engagers deplete tumour-associated macrophages in cancer patient samples. *J. Immunother. Cancer.* **7**, 320-37 (2019).

Downloaded from aacrjournals.org/cancerres/article-pdf/doi/10.1158/0008-5472.CAN-25-5578/3827263/can-25-5578.pdf by University of Washington user on 07 September 2026

15. Sabatino, R., Battistelli, S., Magnani, M., Rossi, L. Preclinical evaluation of an innovative anti-TAM approach based on zoledronate-loaded erythrocytes. *Drug Deliv. Transl. Res.* **8**, 1355-64 (2018).

16. Matlung, H. L., Szilagyi, K., Barclay, N. A., van den Berg, T. K. The CD47-SIRPalpha signaling axis as an innate immune checkpoint in cancer. *Immunol. Rev.* **276**, 145-164 (2017).

17. Kowal, J., Kornete, M., Joyce, J. A. Re-education of macrophages as a therapeutic strategy in cancer. *Immunotherapy* **11**, 677-689 (2019).

18. Yofe, I., Landsberger, T., Yalin, A., Solomon, I., Costoya, C., Demane, D. F., Shah, M., David, E., Borenstein, C., Barboy, O., Matos, I., Peggs, K. S., Quezada, S.A., Amit, I. Anti-CTLA-4 antibodies drive myeloid activation and reprogram the tumor microenvironment through FcγR engagement and type I interferon signaling. *Nat. Cancer* **11**, 1336-1350 (2022).

19. Chryplewicz, A., Scotton, J., Tichet, M., Zomer, A., Shchors, K., Joyce, J. A., Homicsko, K., Hanahan, D. Immunogenic autophagy, reprogrammed macrophages, and remodeled vasculature in glioblastoma triggers tumor immunity. *Cancer Cell* **40**, 1111-1127 (2022).

20. Ao, J. Y., Zhu, X. D., Chai, Z. T., Cai, H., Zhang, Y. Y., Zhang, K. Z., Kong, L. Q., Zhang, N., Ye, B. G., Ma, D. N., Sun, H. C. Colony-Stimulating Factor 1 Receptor Blockade Inhibits Tumor Growth by Altering the Polarization of Tumor-Associated Macrophages in Hepatocellular Carcinoma. *Mol. Cancer Ther*. **16**, 1544-1554 (2017).

21. Fujiwara, T., Yakoub, M. A., Chandler, A., Christ, A. B., Yang, G., Ouerfelli, O., Rajasekhar, V. K., Yoshida, A., Kondo, H., Hata, T., Tazawa, H., Dogan, Y., Moore, M. A. S., Fujiwara, T., Ozaki, T., Purdue, E., Healey, J. H. CSF1/CSF1R Signaling Inhibitor Pexidartinib (PLX3397) Reprograms Tumor-Associated Macrophages and Stimulates T-cell Infiltration in the Sarcoma Microenvironment. *Mol. Cancer Ther*. **20**, 1388-1399 (2021).

22. Beatty, G. L., Chiorean, E. G., Fishman, M. P., Saboury, B., Teitelbaum, U. R., Sun, W., Huhn, R. D., Song, W., Li, D., Sharp, L. L., Torigian, D. A., O'Dwyer, P. J., Vonderheide, R. H. CD40 agonists alter tumor stroma and show efficacy against pancreatic carcinoma in mice and humans. *Science* **331**, 1612-1616 (2011).

23. Gordon, S. R., Maute, R. L., Dulken, B. W., Hutter, G., George, B. M., McCracken, M. N., Gupta, R., Tsai, J. M., Sinha, R., Corey, D., Ring, A. M., Connolly, A. J., Weissman,

Downloaded from aacrjournals.org/cancerres/article-pdf/doi/10.1158/0008-5472.CAN-25-5578/3827263/can-25-5578.pdf by University of Washington user on 07 September 2026

I. L. PD-1 expression by tumour-associated macrophages inhibits phagocytosis and tumour immunity. *Nature* **545**, 495-499 (2017).

24. Georgoudaki, A. M., Prokopec, K. E., Boura, V. F., Hellqvist, E., Sohn, S., Östling, J., Dahan, R., Harris, R. A., Rantalainen, M., Klevebring, D., Sund, M., Brage, S. E., Fuxe, J., Rolny, C., Li, F., Ravetch, J. V., Karlsson, M. C. Reprogramming Tumor-Associated Macrophages by Antibody Targeting Inhibits Cancer Progression and Metastasis. *Cell Rep*. **15**, 2000-2011 (2016).
25. Majeti, R., Chao, M. P, Alizadeh, A. A., Pang, W. W., Jaiswal, S., Gibbs, K. D., van Rooijen, N., Weissman, I. L. CD47 Is an Adverse Prognostic Factor and Therapeutic Antibody Target on Human Acute Myeloid Leukemia Stem Cells. *Cell* **138**, 286-299 (2009).
26. Garcia-Manero, G., Daver, N. G., Xu, J., Chao, M., Trisha Chung, Anderson Tan, Vivian Wang, Andrew Wei, Vyas, P., Sallman, D.A. Magrolimab + azacitidine versus azacitidine + placebo in untreated higher risk (HR) myelodysplastic syndrome (MDS): The phase 3, randomized, ENHANCE study. *J. Clin. Oncol.* **39**, TPS7055-TPS7055 (2021).
27. van Lith, S. A., van den Brand, D., Wallbrecher, R., van Duijnhoven, S. M., Brock, R. and Leenders, W. P. A conjugate of an anti-epidermal growth factor receptor (egfr) vhh and a cell-penetrating peptide drives receptor internalization and blocks egfr activation. *ChemBioChem* **18**, 2390-2394 (2017).
28. Herce, H. D., Schumacher, D., Schneider, A. F., Ludwig, A. K., Mann, F. A., Fillies, M., Kasper, M. A., Reinke, S., Krause, E., Leonhardt, H. and Cardoso, M. C. Cell-permeable nanobodies for targeted immunolabelling and antigen manipulation in living cells. *Nat. Chem.* **9**, 762-771 (2017).
29. Dugal-Tessier, J., Thirumalairajan, S. and Jain, N. Antibody-oligonucleotide conjugates: a twist to antibody-drug conjugates. *J. Clin. Med.* **10**, 838 (2021).
30. Rosen, C. B., Kodal, A. L., Nielsen, J. S., Schaffert, D. H., Scavenius, C., Okholm, A. H., Voigt, N. V., Enghild, J. J., Kjems, J., Tørring, T. and Gothelf, K. V. Template-directed covalent conjugation of DNA to native antibodies, transferrin and other metal-binding proteins. *Nat. Chem.* **6**, 804-809 (2014).
31. Neri D. Antibody-Cytokine Fusions: Versatile Products for the Modulation of Anticancer Immunity. *Cancer Immunol. Res.* **7**, 348–354 (2019).

Downloaded from aacrjournals.org/cancerres/article-pdf/doi/10.1158/0008-5472.CAN-25-5578/3827263/can-25-5578.pdf by University of Washington user on 07 September 2026

32. Lu, Z., Truex, N. L., Melo, M. B., Cheng, Y., Li, N., Irvine, D. J. and Pentelute, B. L. IgG-engineered protective antigen for cytosolic delivery of proteins into cancer cells. *ACS Cent. Sci.* **7**, 365-378 (2021).
33. Xiao, H., Woods, E. C., Vukojicic, P. and Bertozzi, C. R. Precision glycocalyx editing as a strategy for cancer immunotherapy. *Proc. Natl. Acad. Sci. U.S.A.* **113**, 10304-10309 (2016).
34. Zhou, Q. Site-Specific Antibody Conjugation with Payloads beyond Cytotoxins. *Molecules* **28**, 917 (2023).
35. Stark, J.C., Gray, M.A., Ibarlucea-Benitez, I., Lustig, M., Bond, A., Cho, B., Govil, I., Luu, T., Priestley, M.J., Veth, T.S., Errington, W.J., Bruncsics, B., Ribi, M.K., Williams, L.A., Sarkar, C.A., Wisnovsky, S., Riley, N.M., Morrissey, M.A., Valerius, T., Ravetch, J.V., Bertozzi, C.R. Antibody-lectin chimeras for glyco-immune checkpoint blockade. *Nat Biotechnol*. 10.1038/s41587-025-02884-6 (2025).
36. Schmassmann, P., Roux, J., Buck, A., Tatari, N., Hogan, S., Rodrigues Mantuano, N., Wiebolt, R., Wang, J., Lee, S., Snijder, B., Martins, T.A., Ritz, M.F., Shekarian, T., Kaymak, D., McDaid, M., Weller, M, Weiss, T., Läubli, H., Hutter, G. Targeting the Siglec–sialic acid axis promotes antitumor immune responses in preclinical models of glioblastoma. *Sci. Transl. Med. **15**, eadf5302* (2023).
37. Stanczak, M.A., Rodrigues Mantuano, N., Kirchhammer, N., Sanin, D.E., Jacob, F., Coelho, R., Everest-Dass, A.V., Wang, J., Trefny, M.P., Monaco, G. and Bärenwaldt, A. Targeting cancer glycosylation repolarizes tumor-associated macrophages allowing effective immune checkpoint blockade. *Sci. Transl. Med.***14**, eabj1270 (2022).
38. Yang, W., Hicks, D.R., Ghosh, A., Schwartze, T.A., Conventry, B., Goreshnik, I., Allen, A., Halabiya, S.F., Johng Kim, C., Hinck, C.S., Lee, D.S., Bera, A.K., Li, Z., Wang, Y., Schlichthaerle, T., Cao, L., Huang, B. Garrett, S., Gerben, S.R., Rettie, S., Heine, P., Murray, A., Edman, N., Carter, L., Stewart, L., Almo, S., Hinck, A.P., Baker, D. Design of high-affinity binders to immune modulating receptors for cancer immunotherapy. *Nature Comm.* **16**, 2001 (2025).
39. Heeb, L.V., Taskoparan, B., Katsoulas, A., Beffinger, M., Clavien, P.A., Kobold, S., Gupta, A., Berg, J.V. HDR-based CRISPR/Cas9-mediated Knockout of PD-L1 in C57BL/6 Mice. *Bio Protoc.* **13**, e4724. (2023).

Downloaded from aacrjournals.org/cancerres/article-pdf/doi/10.1158/0008-5472.CAN-25-5578/3827263/can-25-5578.pdf by University of Washington user on 07 September 2026

40. Liu, X., Pu, Y., Cron, K., Deng, L., Kline, J., Frazier, W.A., Xu, H., Peng, H., Fu, Y.X., Xu, M.M. CD47 blockade triggers T cell-mediated destruction of immunogenic tumors. *Nat Med*. **21**, 1209-15 (2015).\
41. Huang, B., Abedi, M., Ahn, G., Coventry, B., Sappington, I., Tang, C., Wang, R., Schlichthaerle, T., Zhang, J.Z., Wang, Y., Goreshnik, I., Chiu, C.W., Chazin-Gray, A., Chan, S., Gerben, S., Murray, A., Wang, S., O'Neill, J., Yi, L., Yeh, R., Misquith, A., Wolf, A., Tomasovic, L.M., Piraner, D.I., Duran Gonzalez, M.J., Bennett, N.R., Venkatesh, P., Ahlrichs, M., Dobbins, C., Yang, W., Wang, X., Sahtoe, D.D., Vafeados, D., Mout, R., Shivaei, S., Cao, L., Carter, L., Stewart, L., Spangler, J.B., Roybal, K.T., Greisen, P.J., Li, X., Bernardes, G.J.L., Bertozzi, C.R., Baker, D. Designed endocytosis-inducing proteins degrade targets and amplify signals. *Nature* **638**, 796-804. (2025).
42. Najjar, V. A., Nishioka, K. 'Tuftsin': a natural phagocytosis stimulating peptide. *Nature* **228**, 672-673 (1970).
43. Najjar, V. A. Tuftsin, a natural activator of phagocyte cells: an overview. *Ann. N. Y. Acad. Sci.* **419**, 1-11 (1983).
44. Fridkin, M. and Najjar, V. A. Tuftsin: its chemistry, biology, and clinical potential. *Crit. Rev. Biochem. Mol. Biol.* ***24***, 1-40 (1989).
45. Bar-Shavit, Z., Stabinsky, Y., Fridkin, M. and Goldman, R. Tuftsin-macrophage interaction: Specific binding and augmentation of phagocytosis. *J. Cell. Physiol.* **100**, 55-62 (1979).
46. Nishioka, K., Obeyesekere, N. U. and McMurray, J. S. Enhanced phagocytosis activity of cyclic analogs of tuftsin. *Biochem. Pharmacol.* **49**, 735-738 (1995).
47. von Wronski, M.A., Raju, N., Pillai, R., Bogdan, N.J., Marinelli, E.R., Nanjappan, P., Ramalingam, K., Arunachalam, T., Eaton, S., Linder, K.E., Yan, F., Pochon, S., Tweedle, M.F., Nunn, A.D. Tuftsin binds neuropilin-1 through a sequence similar to that encoded by exon 8 of vascular endothelial growth factor. *J. Biol. Chem*. **281**, 5702-10 (2006).
48. Nissen, J.C., Selwood, D.L., Tsirka, S.E. Tuftsin signals through its receptor neuropilin-1 via the transforming growth factor beta pathway. *J Neurochem.* **127**, 394-402 (2013).
49. Yuan D., Zhai, X., Zhu, K., Ji, J., Liu, W. Tuftsin-tailored fusion protein inhibits the growth of circulating gastric tumor cells associated with macrophage phagocytosis. *Biochem Biophys Rep.* **24**, 101443 (2023).

Downloaded from aacrjournals.org/cancerres/article-pdf/doi/10.1158/0008-5472.CAN-25-5578/3827263/can-25-5578.pdf by University of Washington user on 07 September 2026

50. Zhao, Y., Han, B., Hao, J., Zheng, Y., Chai, J., Zhang, Z., Liu, Z., Shi, L. Bi-specific macrophage nano-engager for cancer immunotherapy. *Nano Today* **41**, 101313 (2021).
51. Liang, D. S., Wen, Z. J., Wang, J. H., Zhu, F. F., Guo, F., Zhou, J. L., Xu, J. J., Zhong, H. J. Legumain protease-sheddable PEGylated, tuftsin-modified nanoparticles for selective targeting to tumour-associated macrophages. *J. Drug Target.* **30**, 82–93 (2022).
52. Fior, R., Póvoa, V., Mendes, R.V., Carvalho, T., Gomes, A., Figueiredo, N., Ferreira, M. G. Single-cell functional and chemosensitive profiling of combinatorial colorectal therapy in zebrafish xenografts. *Proc. Natl. Acad. Sci. U.S.A.* **114**, E8234-E8243 (2017).
53. Fazio, M., Ablain, J., Chuan, Y., Langenau, D. M., Zon, L. I. Zebrafish patient avatars in cancer biology and precision cancer therapy. *Nat. Rev. Cancer* **20**, 263–273 (2020).
54. Rebelo de Almeida, C., Mendes, R. V., Pezzarossa, A., Gago, J., Carvalho, C., Alves, A., Nunes, V., Brito, M. J., Cardoso, M. J., Ribeiro, J., Cardoso, F., Ferreira, M. G., Fior, R. Zebrafish xenografts as a fast screening platform for bevacizumab cancer therapy. *Commun. Biol.* **3**, 299 (2020).
55. Hartley, G. P., Chow, L., Ammons, D. T., Wheat, W. H., Dow, S.W. Programmed cell death ligand 1 (PD-L1) signaling regulates macrophage proliferation and activation. *Cancer Immunol. Res.* **6**, 1260-1273 (2018).
56. Li, W., Wu, F., Zhao, S., Shi, P., Wang, S., Cui, D. Correlation between PD-1/PD-L1 expression and polarization in tumor-associated macrophages: A key player in tumor immunotherapy. *Cytokine Growth Factor Rev.* **67**, 49-57 (2022).
57. Pu, Y., Ji, Q. Tumor-associated macrophages regulate PD-1/PD-L1 immunosuppression. *Front. Immunol.* **13**, 874589. (2022).
58. Xia, Q., Jia, J., Hu, C., Lu, J., Li, J., Xu, H., Fang, J., Feng, D., Wang, L. and Chen, Y. Tumor-associated macrophages promote PD-L1 expression in tumor cells by regulating PKM2 nuclear translocation in pancreatic ductal adenocarcinoma. *Oncogene* **41**, 865-877 (2022).
59. Baranyai, Z., Biri-Kovács, B., Kratky, M., Szeder, B., Debreczeni, M. L., Budai, J., Kovács, B., Horváth, L., Pári, E., Németh, Z., Cervenak, L., Zsila, F., Méhes, E., Kiss, É., Vinšová, J., Bősze, S. Cellular internalization and inhibition capacity of new anti-glioma peptide conjugates: physicochemical characterization and evaluation on

Downloaded from aacrjournals.org/cancerres/article-pdf/doi/10.1158/0008-5472.CAN-25-5578/3827263/can-25-5578.pdf by University of Washington user on 07 September 2026

various monolayer-and 3D-spheroid-based in vitro platforms. *J. Med. Chem.*, **64**, 2982-3005 (2021).

60. Tang, H., Liang, Y., Anders, R.A., Taube, J.M., Qiu, X., Mulgaonkar, A., Liu, X., Harrington, S.M., Guo, J., Xin, Y., Xiong, Y., Nham, K., Silvers, W., Hao, G., Sun, X., Chen, M., Hannan, R., Qiao, J., Dong, H., Peng, H., Fu, Y.X. PD-L1 on host cells is essential for PD-L1 blockade-mediated tumor regression. *J Clin Invest*. **128**, 580-588 (2018).
61. Wells, J. A., Kumru, K. Extracellular targeted protein degradation: an emerging modality for drug discovery. *Nat. Rev. Drug Discov.* **23**, 126-140 (2024).
62. Banik, S. M., Pedram, K., Wisnovsky, S., Ahn, G., Riley, N. M., Bertozzi, C.R. Lysosome-targeting chimaeras for degradation of extracellular proteins. *Nature* **584**, 291-297 (2020).
63. He, W., Chen, C., Zheng, J., Li, Y., Shi, H., Zhou, Y., Li, M., Gong, P., Liu, K., Shao, X., Yao, X., Li, H., Chen, L., Fang, L. Targeted degradation of cell surface proteins through endocytosis triggered by cell-penetrating peptide-small molecule conjugates. *Nat Commun.* **16**, 7575 (2025).
64. Caianiello, D. F., Zhang, M., Ray, J. D., Howell, R. A., Swartzel, J. C., Branham, E. M., Chirkin, E., Sabbasani, V. R., Gong, A. Z., McDonald, D. M. and Muthusamy, V. Bifunctional small molecules that mediate the degradation of extracellular proteins. *Nat. Chem. Biol.* **17**, 947-953 (2021).
65. Wang, T., Sun, L., Ren, T., Hou, M., Long, Y., Jiang, J. H., He, J. Targeted Protein Degradation Mediated by Genetically Engineered Lysosome-Targeting Exosomes. *Nano Lett.* ***23***, 9571-9578 (2023).
66. Siriwardena, S. U., Munkanatta Godage, D. N., Shoba, V. M., Lai, S., Shi, M., Wu, P., Chaudhary, S. K., Schreiber, S. L. and Choudhary, A. Phosphorylation-inducing chimeric small molecules. *J. Am. Chem. Soc.* **142**, 14052-14057 (2020).
67. Casey, S.C., Tong, L., Li, Y., Do, R., Walz, S., Fitzgerald, K.N., Gouw, A.M., Baylot, V., Gütgemann, I., Eilers, M., Felsher, D.W. MYC regulates the antitumor immune response through CD47 and PD-L1. *Science* **352**, 227-31 (2016).
68. Liu, X., Liu, L., Ren, Z., Yang, K., Xu, H., Luan, Y., Fu, K., Guo, J., Peng, H., Zhu, M., Fu, Y.X. Dual Targeting of Innate and Adaptive Checkpoints on Tumor Cells Limits Immune Evasion. *Cell Reports*. **24**, 2101-2111 (2018).

Downloaded from aacrjournals.org/cancerres/article-pdf/doi/10.1158/0008-5472.CAN-25-5578/3827263/can-25-5578.pdf by University of Washington user on 07 September 2026

69. Liu, X., Pu, Y., Cron, K., Deng, L., Kline, J., Frazier, W.A., Xu, H., Peng, H., Fu, Y.X., Xu, M.M. CD47 blockade triggers T cell-mediated destruction of immunogenic tumors. *Nat. Medicine*. **21**, 1209-15 (2015).
70. Juneja, V.R., McGuire, K.A., Manguso, R.T., LaFleur, M.W., Collins, N., Haining, W.N., Freeman, G.J., Sharpe, A.H. PD-L1 on tumor cells is sufficient for immune evasion in immunogenic tumors and inhibits CD8 T cell cytotoxicity. *J. Exp. Med.* **3**, 895-904 (2017).
71. Jacobs, S. A., Gibbs, A.C., Conk, M., Yi, F., Maguire, D., Kane, C., O'Neil, K. T. Fusion to a highly stable consensus albumin binding domain allows for tunable pharmacokinetics. *Protein Eng Des Sel.* **28**, 385-393 (2015).
72. Torphy, R.J., Zhu, Y., Schulick, R.D. Immunotherapy for pancreatic cancer: Barriers and breakthroughs. *Ann Gastroenterol Surg*. **2**, 274-281 (2018).
73. Clark, C.E., Hingorani, S.R., Mick, R., Combs, C., Tuveson, D.A., Vonderheide, R.H. Dynamics of the immune reaction to pancreatic cancer from inception to invasion. *Cancer Res.* **67**, 9518-9527 (2007).
74. Zhang, Y., Velez-Delgado, A., Mathew, E., Li, D., Mendez, F.M., Flannagan, K., Rhim, A.D., Simeone, D.M., Beaty, G.L., Pasca di Magliano, M. Myeloid cells are required for PD-1/PD-L1 checkpoint activation and the establishment of an immunosuppressive environment in pancreatic cancer. *Gut*. **66**, 124-136 (2017).
75. Westphalen, C.B., Olive, K.P. Genetically engineered mouse models of pancreatic cancer. *Cancer J*. **18**, 502-510 (2012).

Downloaded from aacrjournals.org/cancerres/article-pdf/doi/10.1158/0008-5472.CAN-25-5578/3827263/can-25-5578.pdf by University of Washington user on 07 September 2026

Figure Legends

Figure 1. Synthesis, characterization and functional PD-L1 binding of the PSEs.

a, Schematic of a phagocytic synapse enhancer (PSE) consisting of a de novo PD-L1 binder, PEG linker, and an immunomodulating peptide (tuftsin) designed to engage simultaneously macrophage and cancer cell in the TME. Created in BioRender. Sabatino, V. (2026) https://BioRender.com/ix948w7. **b**, The binder ($_{dn}$PDL1) is a cysteine-bearing mini protein with high affinity for PD-L1 conjugated to a maleimide-$_{n}$PEG$_3$-Tuftsin to yield the PSE. Created in BioRender. Sabatino, V. (2026) https://BioRender.com/ep30wix. **c,** Characterization of ^{short}PSE and **d,** ^{long}PSE by LC-MS and PD-L1 binding assays by biolayer interferometry. Dissociation constants are calculated by non-linear regression analysis (^{short}PSE: K_D = 5.7 nM; ^{long}PSE K_D = 5.8 nM). Created in BioRender. Sabatino, V. (2026) https://BioRender.com/ep30wix. **e,** Structure of a FITC-maleimide probe displaying the TKPR peptide for the synthesis of ^{FITC}PSE. Created in BioRender. Sabatino, V. (2026) https://BioRender.com/ep30wix. **f,** PD-L1 expression on MC-38 cells in the absence or presence of IFNγ. Histograms of the probe ^{FITC}PSE bound to MC-38 cells determined by flow cytometry. Cells pre-treated with IFNγ upregulate PD-L1 causing higher shift in fluorescence intensity of the bound ^{FITC}PSE. Created in BioRender. Sabatino, V. (2026) https://BioRender.com/9ciw9rz.

Figure 2. Mϕ-stimulating peptide tuftsin acts via NRP-1 and triggers the PSE-mediated pro-inflammatory phenotype

a, Schematic representation of the tuftsin-mediated uptake of a fluorescent protein. Neutravidin Oregon Green$_{488}$ (NOG$_{488}$) is complexed to the biotinylated peptide (Biot-TKPR), enhancing fluorescent uptake in RAW 264.7 Mϕ. Created in BioRender. Sabatino, V. (2026) https://BioRender.com/9ciw9rz. **b**, Microscopy images of fluorescence uptake. From left to right: NOG$_{488}$, NOG$_{488}$-Biot-TKPR (10, 20, 50 μM). Scale bar: 5 μm. Created in BioRender. Sabatino, V. (2026) https://BioRender.com/9ciw9rz. **c,** Relative quantitative analysis of the mean fluorescence intensity (MFI) of intracellular NOG$_{488}$. (NOG$_{488}$ vs Biot-TKPR 10 μM: p=0.3016; NOG$_{488}$ vs Biot-TKPR 20 μM: p=0.0007; NOG$_{488}$ vs Biot-TKPR 50 μM: p<0.0001). **d,** BLI analysis displaying the binding curves to NRP1 with Peptide (62.5-2,000 nM, K_D = 102 nM), **e,** ^{long}PSE (6.25-100 nM, K_D = 75 nM) and **f,** $_{dn}$PDL1 (3.9-

Downloaded from aacrjournals.org/cancerres/article-pdf/doi/10.1158/0008-5472.CAN-25-5578/3827263/can-25-5578.pdf by University of Washington user on 07 September 2026

4,000 nM, K_D = n/a). Sensorgrams were reference-subtracted and globally fitted to a 1:1 Langmuir binding model using GatorOne software (v2.10.4) to derive kinetic parameters (k_{on}, k_{off}) and the equilibrium dissociation constant (K_D). **g,** schematic of monocyte-derived macrophages (MDMs) treated for 24 hours with ^{long}PSE and subjected to flow cytometry and cytokine analysis. Created in BioRender. Sabatino, V. (2026) https://BioRender.com/9ciw9rz. **h,** Bar graphs display the surface markers (PD-L1, MHC-II, CD86, CD163, NRP1, CD206) expression levels of PSE-treated macrophages vs control (Log2FC, p-values for each marker are displayed on the graph). **i,** Bar graphs display cytokine and chemokine analysis of the supernatant of PSE-treated macrophages vs control (Log2FC CCL2 p= 0.029; CCL3, p=0.0001; CCL5, p<0.0001; CXCL1, p=0.049; CXCL10, p=0.003; IL-1ra, p=0.029; TNFα, p= 0.001; IL-6, p=0.001; IL-8, p=0.255; MIF, p=0.046; Nexin, p=0.001). Statistical analysis was performed on Prism v10 using one sample t and Wilcoxon test.

Figure 3. PSEs mediate the endocytosis of membrane and soluble extracellular target proteins in macrophages

a, Imaging analysis and co-localization studies of PD-L1+ Mϕ treated with ^{FITC}PSE. Created in BioRender. Sabatino, V. (2026) https://BioRender.com/ml06lft. **b,** Single-cell imaging at 30 min and 4h after. Cells were pre-treated with Lysobrite Red (lysosomes), treated with ^{FITC}PSE and post-stained with anti-PD-L1-APC. Displayed channels include: brightfield (grey, cells), FITC (green, ^{FITC}PSE), Lysobrite (yellow, lysosomes), APC (red, PD-L1), and a green/yellow/red merge. **c,** Bright Detail Similarity (BDS) histograms (IDEAS 6.2 software) quantifying colocalization between ^{FITC}PSE and Lysobrite. At 30 min (top, blue), a low peak BDS (~1.0) indicates minimal spatial correlation. By 4 h (bottom, red), the peak shifts right (~1.8), demonstrating high correlation. **d,** Flow cytometric analysis of PD-L1$^+$ THP-1 Mϕ . PD-L1 staining was measured by the MFI of APC$^+$ Mϕ and normalised to the fluorescence of untreated APC$^+$ cells (control). (Control vs Peptide: ns, Control vs $_{dn}$PDL1: p=0.0003, Control vs ^{long}PSE: p<0.0001, n=3). **e,** Co-localization analysis of PD-L1$^+$ THP-1 Mϕ treated with: Media, $_{dn}$PDL1, ^{long}PSE. Bar graphs represent the percentage of co-localized dyes measured by the BDS score of double positive Mϕ (Lysobrite$^+$APC$^+$). Quantitative analysis was performed on IDEAS 6.2 software. **f,** Representative flow cytometric images of PD-L1$^+$ THP-1 Mϕ after 4h treatment with ^{long}PSE (100 nM). Mϕ were stained

Downloaded from aacrjournals.org/cancerres/article-pdf/doi/10.1158/0008-5472.CAN-25-5578/3827263/can-25-5578.pdf by University of Washington user on 07 September 2026

with aPDL1-APC after treatment. Cells were pre-gated as live single cells. From left to right, each image displays channels for Brightfield (BF), Lysobrite Red (lysosome stain), APC (aPD-L1-APC), Lysobrite/APC (merged). Scale bar: 10 μm. Image analysis was performed on IDEAS 6.2 software.

g, Schematic representation for the enhanced uptake of extracellular PD-L1 PSE-mediated. NOG-PDL1 is bound by the PSE, which triggers uptake in Mϕ determined by increased fluorescence intensity of the chromophore. Created in BioRender. Sabatino, V. (2026) https://BioRender.com/9ciw9rz. **h,** Confocal analysis of the enhanced uptake. Panels from left to right display: RAW 264.7 Mϕ treated with NOG_{488}; NOG-PDL1 + $_{dn}$PDL1; NOG-PDL1 + $_{dn}$PDL1 + tuftsin; NOG-PDL1 + ^{long}PSE. Images contain the merged channels of i) blue channel – DAPI (nuclei); ii) green channel – NOG_{488}. Created in BioRender. Sabatino, V. (2026) https://BioRender.com/9ciw9rz. **i,** Quantitative fluorescence measurements of the intracellular uptake of the complex NOG_{488}-PDL1. (NOG-PDL1 + $_{dn}$PDL1 vs NOG-PDL1 + ^{long}PSE: $p<0.0001$, NOG-PDL1 + $_{dn}$PDL1 vs NOG-PDL1 + $_{dn}$PDL1 + Peptide: $p=0.0089$, NOG-PDL1 + $_{dn}$PDL1 + Peptide vs ^{long}PSE: $p=0.0014$). The average MFI was calculated by processing the images on QuPath. Statistical analysis was performed on Prism v10 using ordinary one-way ANOVAs, followed by Tukey's multiple comparison test to compare treatment groups. In every instance, the asterisk * indicates a $p<0.05$, ** indicates $p<0.01$, *** indicates $p<0.001$, and **** indicates $p<0.0001$.

Figure 4. PSEs boost avidity and phagocytic activity in co-cultures and extend overall survival in the CRC syngeneic model.

a, Schematic representation of effector-target cell interaction and increase in avidity triggered by PSEs. PSEs (125 nM) with different linker lengths were incubated for 3 min in co-culture before application of acoustic force (0 to 1000 pN). Avidity assays show overall increased avidity with the PSEs compared to the control Peptide (n=4). Statistical analysis was performed using unpaired two-tailed t test to compare PSEs to control Peptide. Created in BioRender. Sabatino, V. (2026) https://BioRender.com/8rwthy1. **b,** Confocal imaging of co-culture assays. RAW 264.7 Mϕ (stained with CMFDA green) were co-cultured with MC-38 cancer cells (stained with CellTrace Far Red proliferation kit) and treated for 4h with the respective

Downloaded from aacrjournals.org/cancerres/article-pdf/doi/10.1158/0008-5472.CAN-25-5578/3827263/can-25-5578.pdf by University of Washington user on 07 September 2026

molecules. Panels (A-C) correspond to co-cultures treated respectively with: Peptide, ^{short}PSE, ^{long}PSE. Scale bar: 100 μm. **c,** Flow Cytometric analysis after 4h incubation with different PSEs and controls showed an increase in the amount of double-positive PE^+ $APC750^+$ Mϕ. Cells were co-cultured in 1:1 ratio in tissue culture-treated 96-well plates. (Control vs ^{short}PSE: p=0.0087; linear peptide vs ^{long}PSE: p<0.0001, n = 8 or 12). **d,** Phagocytic index of RAW 264.7 Mϕ in co-culture with MC-38 cells treated with the PSEs. The molecules were tested in co-culture (1:1 ratio) during 4h incubation. To determine the phagocytic index, double-positive Mϕ were pre-gated as PE^+ Mϕ. **e,** FC analysis after 4h incubation with different concentrations of PSE. Cells were co-cultured in a 1:1 ratio in tissue culture-treated 96-well plates. ($_{dn}$PDL1 vs 1 μM ^{long}PSE: p=0.0008; $_{dn}$PDL1 vs 100 nM PSE: p=0.0004, $_{dn}$PDL1 vs Control: p=0.0082; peptide vs 1 μM ^{long}PSE: p<0.0001, n = 4). Gating strategy and representative histograms for each condition are shown. **f,** FC analysis after 2h incubation of ^{long}PSE or Magrolimab as benchmark control. Phagocytic index (%) is shown as the amount of double-positive PE^+ $APC750^+$ Mϕ pre-gated on PE^+ Mϕ. Assay medium is used as a control. Cells were co-cultured in 1:1 ratio in tissue culture-treated 96-well plates. (Control vs PSE: p<0.0001; Control vs Magrolimab: p<0.0001; n = 8 or 12). Representative histograms for each condition are shown. **g,** Experimental design of the *in vivo* study with a syngeneic model of CRC. $1x10^6$ MC-38 tumor cells were inoculated subcutaneously into C57BL/6J mice on d 0. Then, different treatments (^{long}PSE, $_{dn}$PDL1, peptide, Magrolimab, or PBS) (n=6 per group) were administered i.t. on d7, 10, and 13. Mice were sacrificed when tumor volume reached ~1000 mm^3. Created in BioRender. Sabatino, V. (2026) https://BioRender.com/v17d531. **h,** body weight changes during treatment with ^{long}PSE, peptide, $_{dn}$PDL1, Magrolimab, and vehicle (PBS). The body weight of each group of mice was measured every day; **i,** tumor growth curve. Data represent mean ± SEM of n=6. Multiple unpaired t-test. *p<0.05; **j,** overall survival of treated mice. Log-rank (Mantel-Cox) test indicates a statistically significant difference between the treated mice and the vehicle group. (PBS vs ^{long}PSE: p=0.001; Peptide: p=0.0095; Magrolimab: p=0.0036).

Figure 5. Half-life extended PSEs improve survival of CRC-bearing mice by intratumoral or intravenous injections.

Downloaded from aacrjournals.org/cancerres/article-pdf/doi/10.1158/0008-5472.CAN-25-5578/3827263/can-25-5578.pdf by University of Washington user on 07 September 2026

a, Fusion protein ABD-$_{dn}$PDL1 with extended half-life ($t_{1/2}$ ~12h) is used for the synthesis of the bifunctional ABD-^{long}PSE. Created in BioRender. Sabatino, V. (2026) https://BioRender.com/t97aa2l. **b,** SDS-PAGE of ^{long}PSE, ABD-^{long}PSE, and their respective unconjugated binders $_{dn}$PDL1 and ABD-$_{dn}$PDL1. **c,** Competition assay with PD-L1^{+} cancer cells (MDA-MB-231). All molecules ($_{dn}$PDL1, ABD-$_{dn}$PDL1, ^{long}PSE, ABD-^{long}PSE) were used in a concentration range (1000-0 nM) together with a fixed concentration of APC-conjugated PD-L1 antibody. **d,** PD-1/PD-L1 blockade assay schematic: Jurkat T cells expressing PD-1 and a luciferase reporter driven by NFAT) are co-cultured with target cells, CHO-K1, expressing PD-L1 and a TCR activator. The PD-1/PD-L1 interaction inhibits T cell activation resulting in low luminescence (left panel). In the presence of a blocking antibody, inhibition of PD-1/PD-L1 axis allows the TCR signaling pathway to activate NFAT and trigger the expression of luciferase (right panel). Created in BioRender. Sabatino, V. (2026) https://BioRender.com/va3kxl3. **e,** Relative Potency curves of PD-L1 blockers. The Y-axis represents Relative Light Units (RLU) generated by the luciferase signal. The X-axis represents the drug concentration. Atezolizumab: EC_{50}=0.294, ABD-^{long}PSE: EC_{50}=2.346, ABD-$_{dn}$PDL1: EC_{50}=2.352. Luminescence was measured as Relative Light Units (RLU) using a Synergy H1 multi-mode microplate reader (BioTek). Data were analyzed using GraphPad Prism software v10. The dose-response curves were generated by plotting the RLU against the $\log_{10}$ of the effector concentration, and EC_{50} values were determined using a non-linear regression (three-parameter logistic fit) model.

f, i.t. treatment of CRC-bearing mice. Tumor cells were inoculated subcutaneously onto C57BL/6J mice on d 0. Then, different treatments (^{long}PSE, ABD-^{long}PSE, $_{dn}$PDL1, ABD-$_{dn}$PDL1, Peptide, Magrolimab or PBS, n=6 per group) were administered i.t. on d7, 9, 11, and 13. Mice were sacrificed when tumor volume reached ~1000 mm^3. Left panel (*i*): body weight change was measured daily during the treatment period. middle panel (*ii*): tumor growth curve. Data represent mean ± SEM of n=6. Multiple unpaired t-test. (PBS vs ^{long}PSE: $p<0.05$; PBS vs ABD-^{long}PSE: $p<0.01$; right panel (*iii*): overall survival of treated mice. Log-rank (Mantel-Cox) test with statistically significant differences between the treated mice and the control group: PBS vs ABD-^{long}PSE: p=0.0008; ABD-$_{dn}$PDL1: p=0.0061; ^{long}PSE: p=0.0008; $_{dn}$PDL1: p=0.029; Magrolimab: p=0.0055; Peptide: p=0.1765. Created in BioRender. Sabatino, V. (2026) https://BioRender.com/v17d531. **g,** i.v. treatment of CRC-bearing mice, from left to right, *i*) body weight changes during treatment with ABD-^{long}PSE, ABD-$_{dn}$PDL1,

Downloaded from aacrjournals.org/cancerres/article-pdf/doi/10.1158/0008-5472.CAN-25-5578/3827263/can-25-5578.pdf by University of Washington user on 07 September 2026

Peptide, Vehicle (PBS). The body weight of each group of mice was measured every day; *ii*) tumor growth curve. Data represent mean ± SEM of n=6. Multiple unpaired t-test. PBS vs ABD-^{long}PSE: p=0.049; *iii*) overall survival of treated mice. Statistical analysis performed with Log-rank test (PBS vs ABD-^{long}PSE: p=0.0033).

Figure 6. PSE-treatment improves survival in an orthotopic model of pancreatic cancer and leads to immune modulation of the TME.

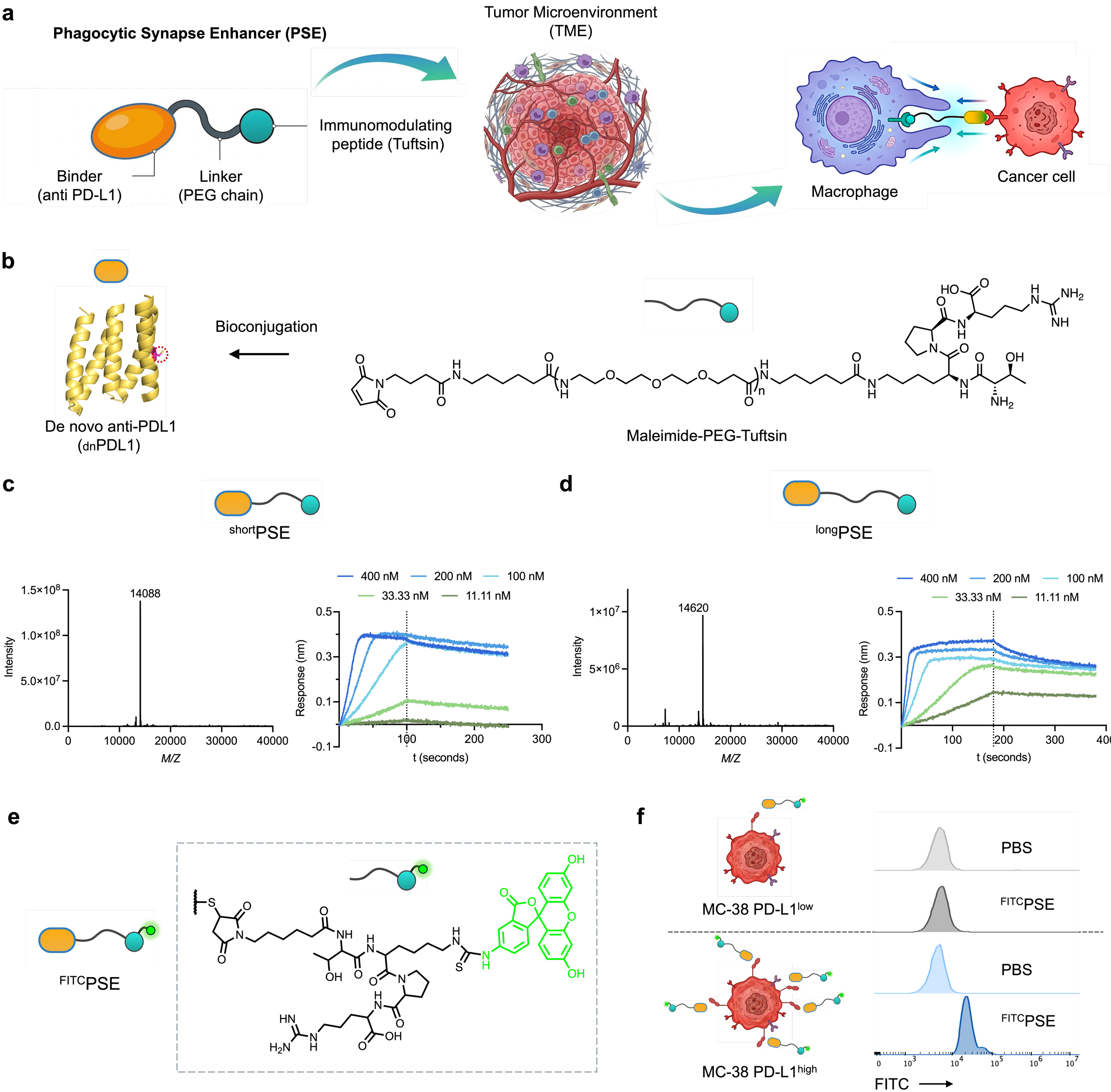
a, KPC cells were inoculated orthotopically into C57BL/6J mouse pancreas on d 0. Treatments (ABD-^{long}PSE, ABD-$_{dn}$PDL1, Peptide, Magrolimab or PBS, n=10 per group) were administered i.v. on d5, 7, 9 and 12. At d15, 4 mice/group were sacrificed for tumor immune profiling, while the remaining 6 mice/group were kept for survival analysis. Created in BioRender. Sabatino, V. (2026) https://BioRender.com/svswoel. **b,** Panels from left to right, *i*) Analysis of tumor burden at d15 using unpaired two-tailed t test. (PBS vs ABD-^{long}PSE: p=0.011). Data represent mean ± SEM of n=4; *ii*) Daily body weight changes during treatment with ABD-^{long}PSE, ABD-$_{dn}$PDL1, Peptide, Magrolimab, Vehicle (PBS); *iii*) Overall survival analysis. Log-rank (Mantel-Cox) test statistical analysis of treatment vs control group (n=6): PBS vs ABD-^{long}PSE: p=0.0002. **c,** Flow cytometric analysis of the lymphoid compartment. Upper panels, percent of live cells from left to right: *i*) CD45$^+$ (Vehicle vs Magrolimab p=0.005; Vehicle vs ABD-^{long}PSE p=0.066), *ii*) T cells (CD45$^+$CD3$^+$, Magrolimab vs ABD-^{long}PSE p=0.03), *iii*) T regs (CD45$^+$CD3$^+$CD4$^+$CD25$^+$FoxP3$^+$, Vehicle vs ABD-$_{dn}$PDL1 p=0.037, Vehicle vs ABD-^{long}PSE p=0.005, Vehicle vs Peptide p=0.021); *iv*) NK cells (CD45$^+$ NK1.1$^+$, Vehicle vs Magrolimab p=0.042, Vehicle vs ABD-^{long}PSE p=0.056); lower panels, from left to right: *v*) CD4 T cells (CD45$^+$CD3$^+$CD4$^+$), *vi*) CD8 T cells (CD45$^+$CD3$^+$CD8$^+$), *vii*) PD-1$^+$ CD4 T cells (CD45$^+$CD3$^+$CD4$^+$PD-1$^+$, Magrolimab vs ABD-$_{dn}$PDL1 p=0.026, ABD-$_{dn}$PDL1 vs ABD-^{long}PSE p=0.004) *viii*) PD-1$^+$ CD8 T cells (CD45$^+$CD3$^+$CD4$^+$PD-1$^+$, ABD-^{long}PSE vs ABD-$_{dn}$PDL1 p=0.04, Vehicle vs ABD-^{long}PSE p=0.01). **d,** Flow cytometric analysis of myeloid cells. Upper panels: percent of live cells from left to right: *i*) Neutrophils/MDSCs (CD45$^+$CD11b$^+$Ly6G$^+$, Vehicle vs ABD-^{long}PSE p=0.0005), *ii*) DCs (CD45$^+$CD11b$^+$CD11c$^+$MHCII$^+$), *iii*) CD103$^+$ DCs (Vehicle vs ABD-^{long}PSE p=0.015); *iv*) PDL1$^+$ DCs (CD45$^+$CD11b$^+$CD11c$^+$MHCII$^+$PD-L1$^+$, Vehicle vs ABD-$_{dn}$PDL1 p=0.006, ABD-$_{dn}$PDL1 vs ABD-^{long}PSE p=0.043). Lower panels: percent of live cells from left to right: *v*) TAMs (CD45$^+$CD11b$^+$F4-80$^+$, Vehicle vs ABD-^{long}PSE: p=0.001; Magrolimab vs ABD-^{long}PSE: p=0.008), *vi*) CD206+ TAMs

Downloaded from aacrjournals.org/cancerres/article-pdf/doi/10.1158/0008-5472.CAN-25-5578/3827263/can-25-5578.pdf by University of Washington user on 07 September 2026

($CD45^+CD11b^+F4\text{-}80^+CD206^+$,Vehicle vs ABD-$_{dn}$PDL1 p=0.007, Vehicle vs ABD-^{long}PSE p=0.012), *vii*) MFI PD-L1$^+$ TAMs ($CD45^+CD11b^+F4\text{-}80^+PD\text{-}L1^+$, ABD-^{long}PSE vs ABD-$_{dn}$PDL1 p=0.0004, ABD-$_{dn}$PDL1 vs Peptide p=0.0007) *viii*) MFI CD80$^+$ TAMs ($CD45^+CD11b^+F4\text{-}80^+CD80^+$, Vehicle vs ABD-^{long}PSE: p=0.002). Statistical analysis was performed using unpaired t test to compare treatments to Vehicle or ordinary one-way ANOVAs followed by Tukey's multiple comparison test to compare all treatment groups.

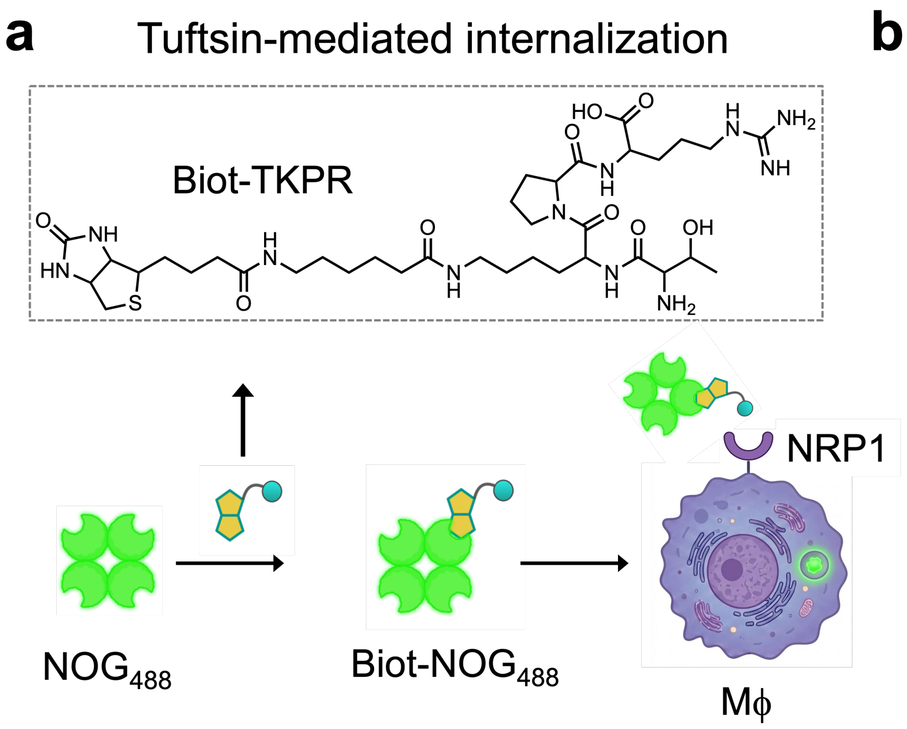
Downloaded from aacrjournals.org/cancerres/article-pdf/doi/10.1158/0008-5472.CAN-25-5578/3827263/can-25-5578.pdf by University of Washington user on 07 September 2026

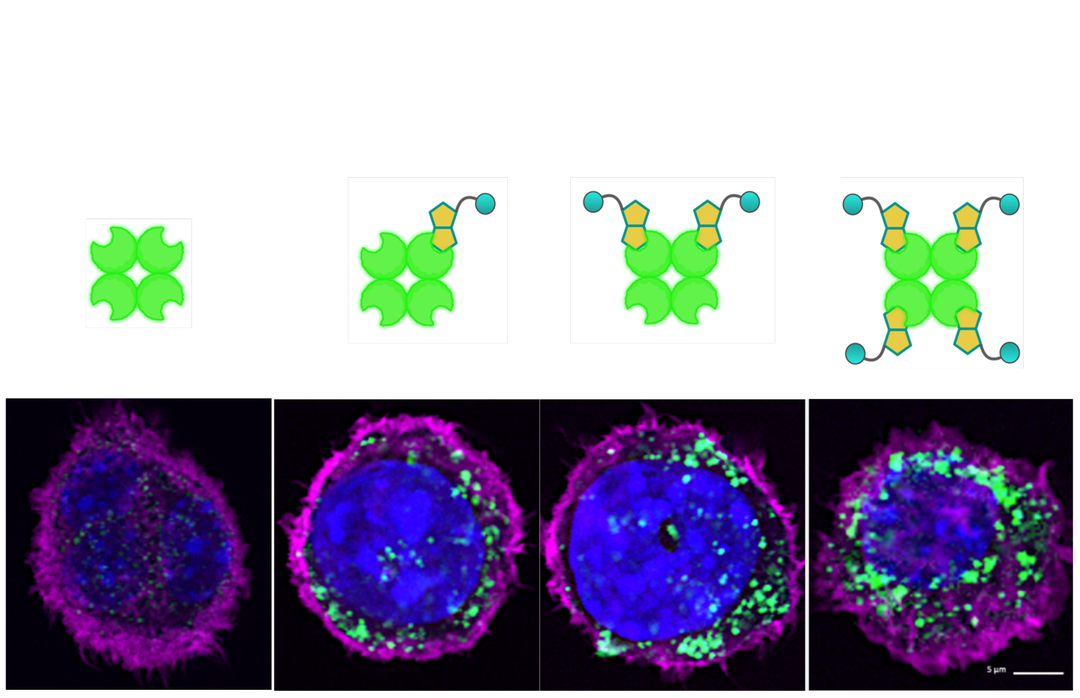
FIGURE 1

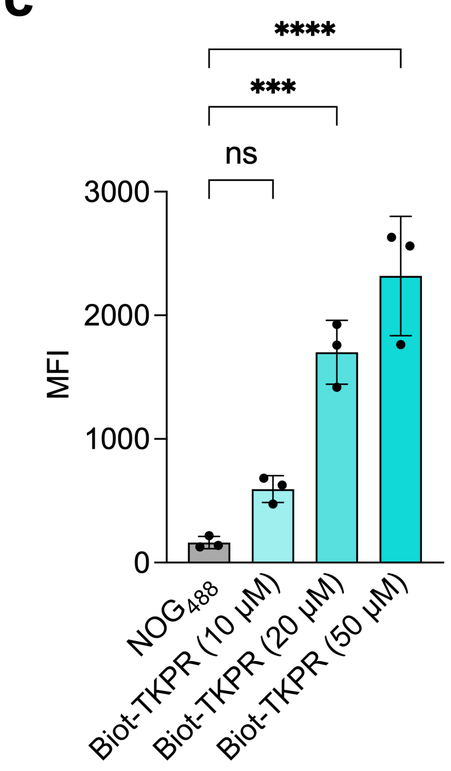


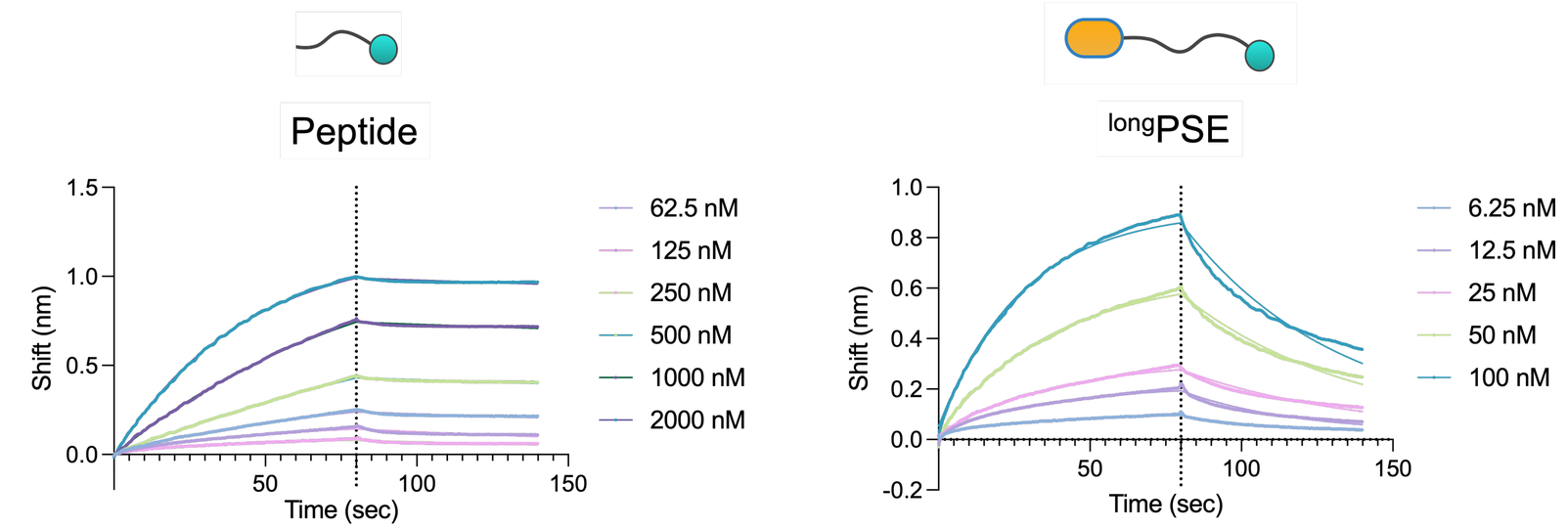
Downloaded from aacrjournals.org/cancerres/article-pdf/doi/10.1158/0008-5472.CAN-25-5578/3827283/can-25-5578.pdf by University of Washington user on 07 September 2026

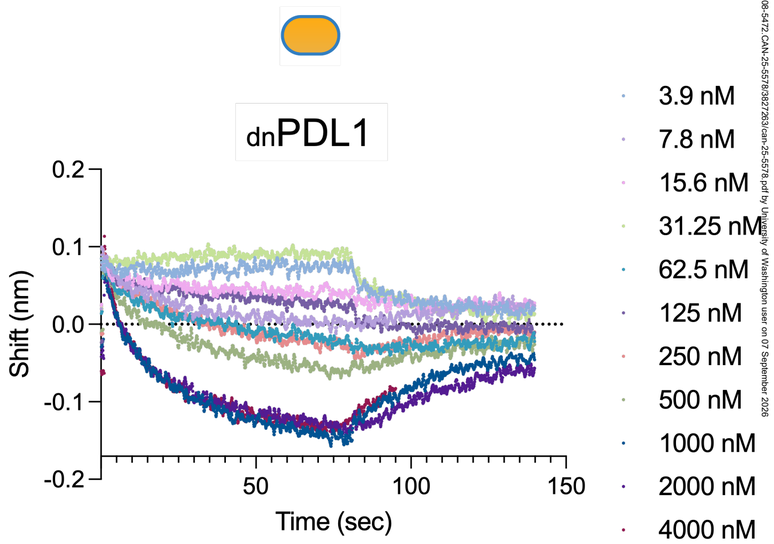
FIGURE 2

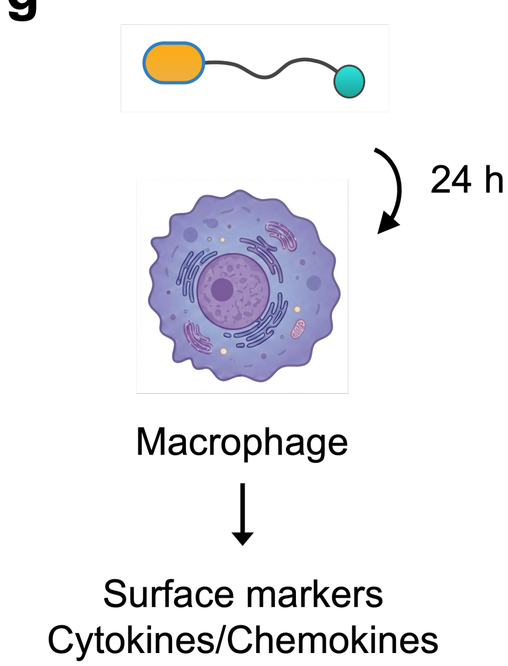


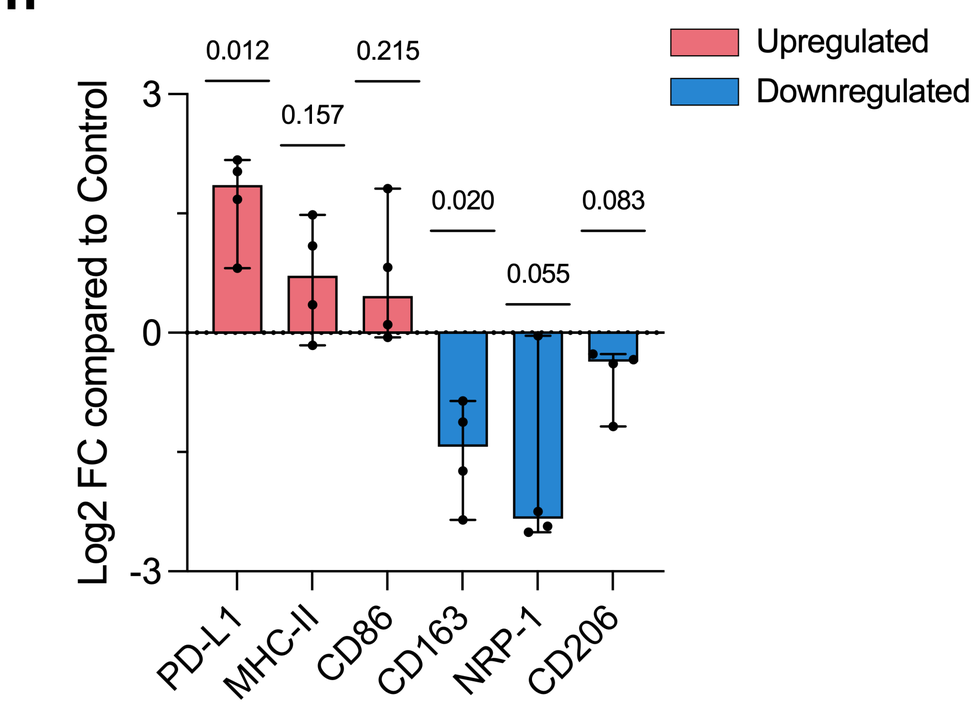


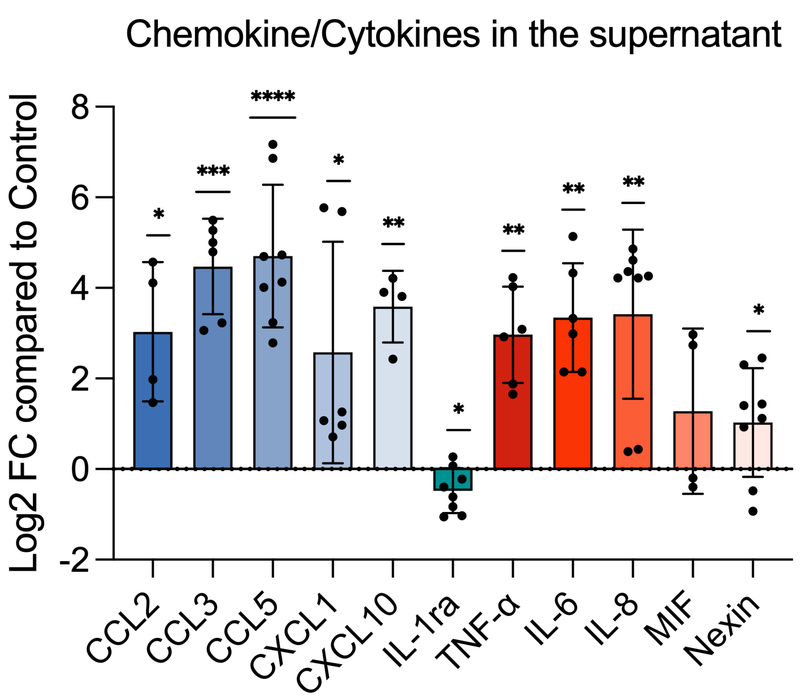






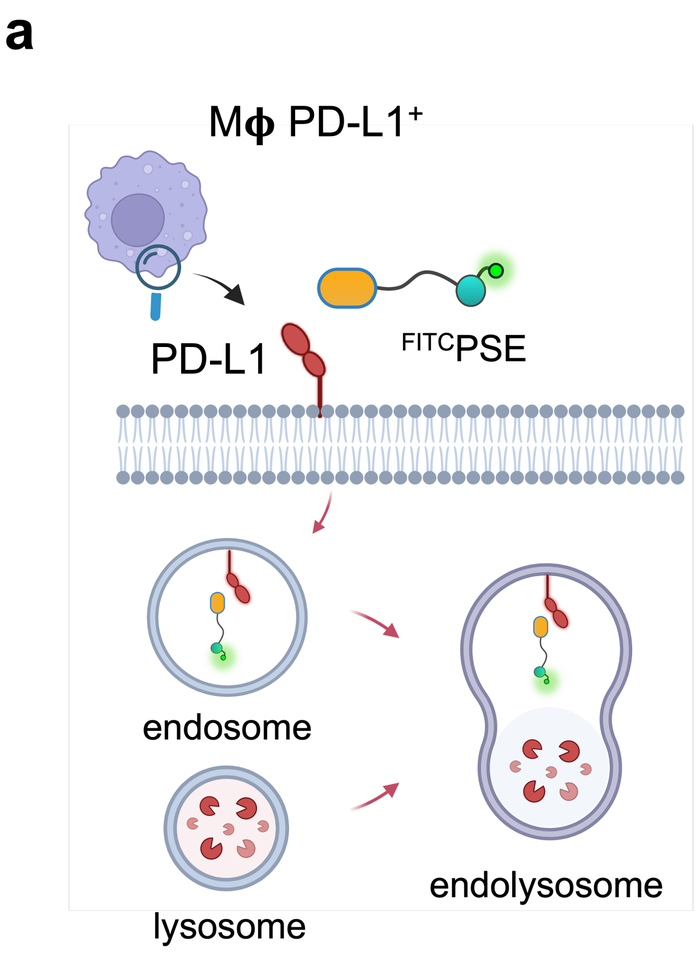


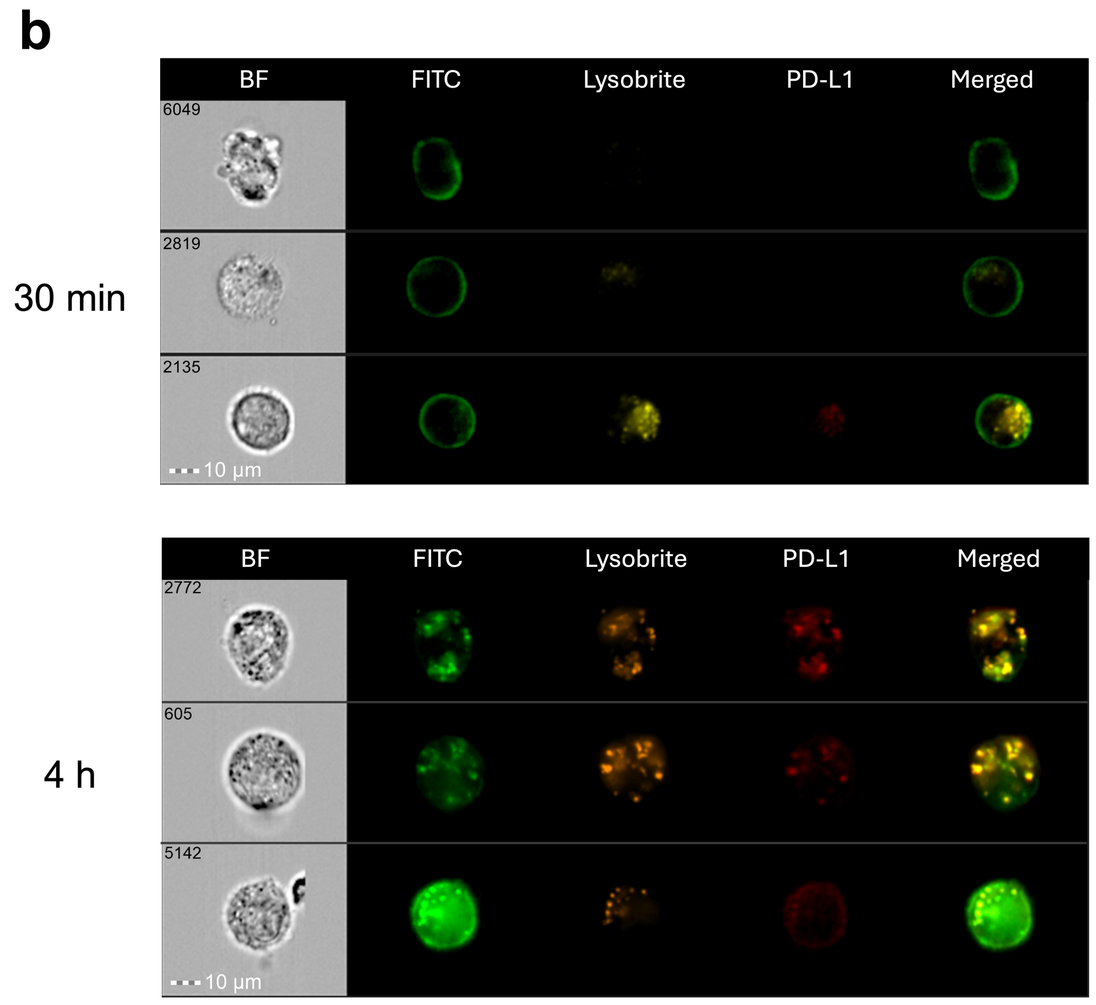


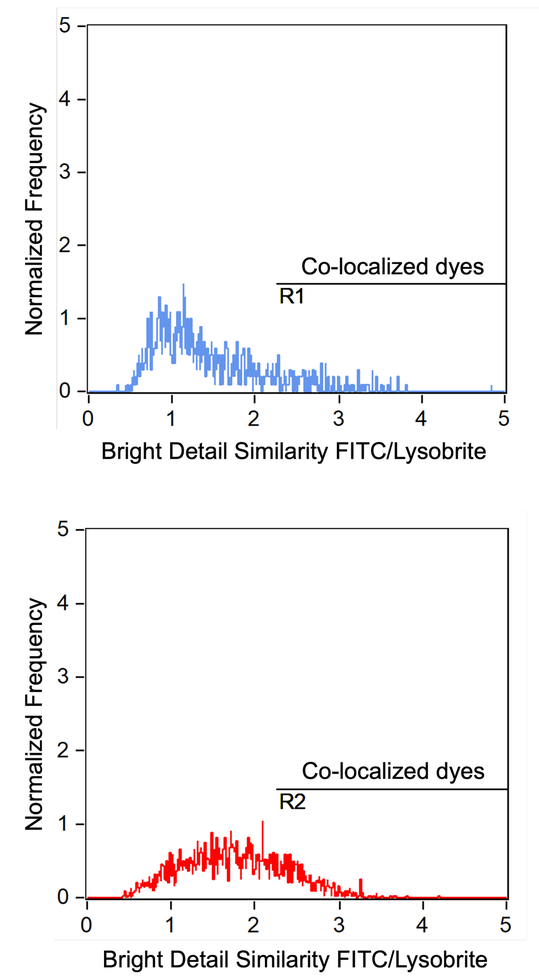


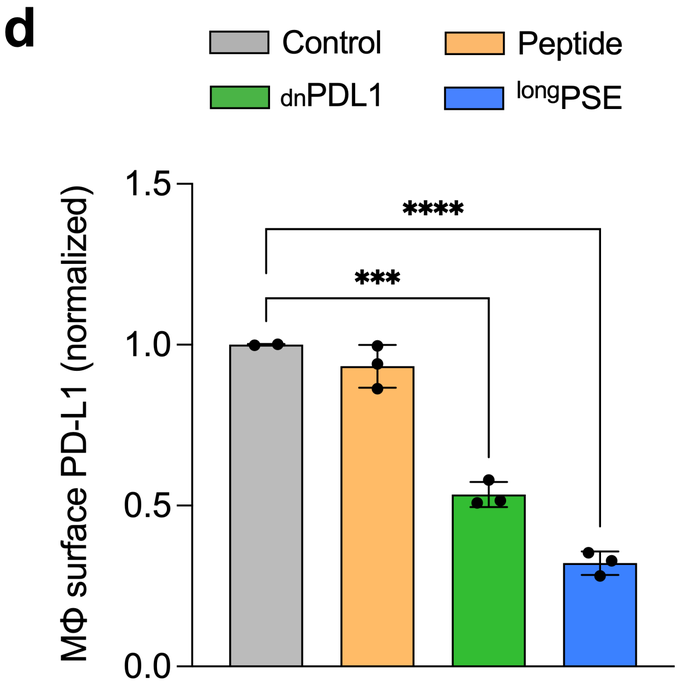
Downloaded from aacrjournals.org/cancerres/article-pdf/doi/10.1158/0008-5472.CAN-25-55
7863827263/can-25-5578.pdf by University of Washington user on 07 September 2026

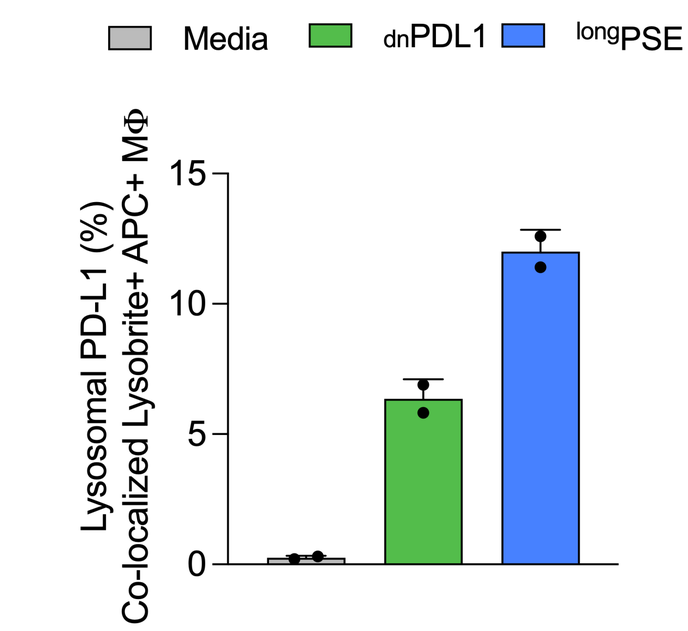
FIGURE 3

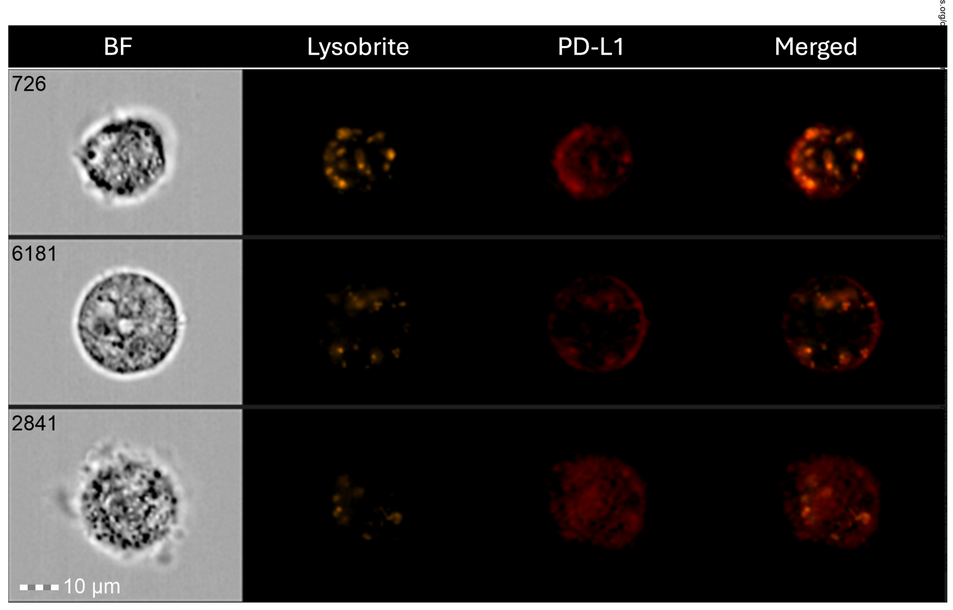

a
MΦ PD-L1+
PD-L1
FITCPSE
endosome
endolysosome
lysosome

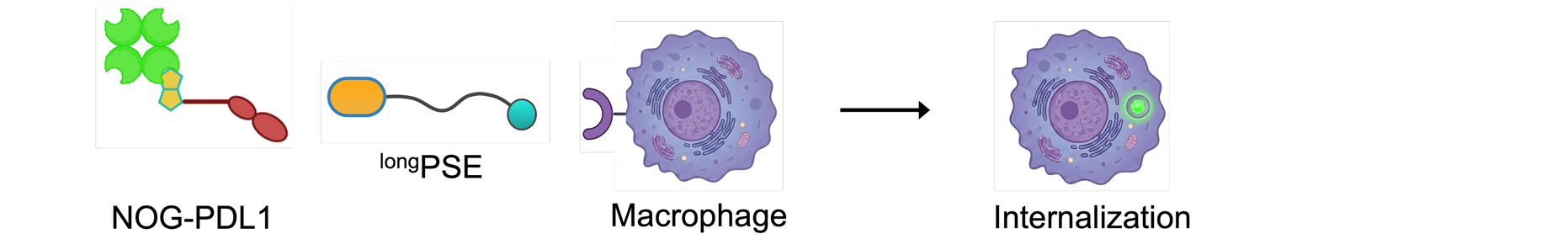

b
BF
FITC
Lysobrite
PD-L1
Merged
30 min
6049
2819
2135
10 µm
4 h
2772
605
5142
10 µm

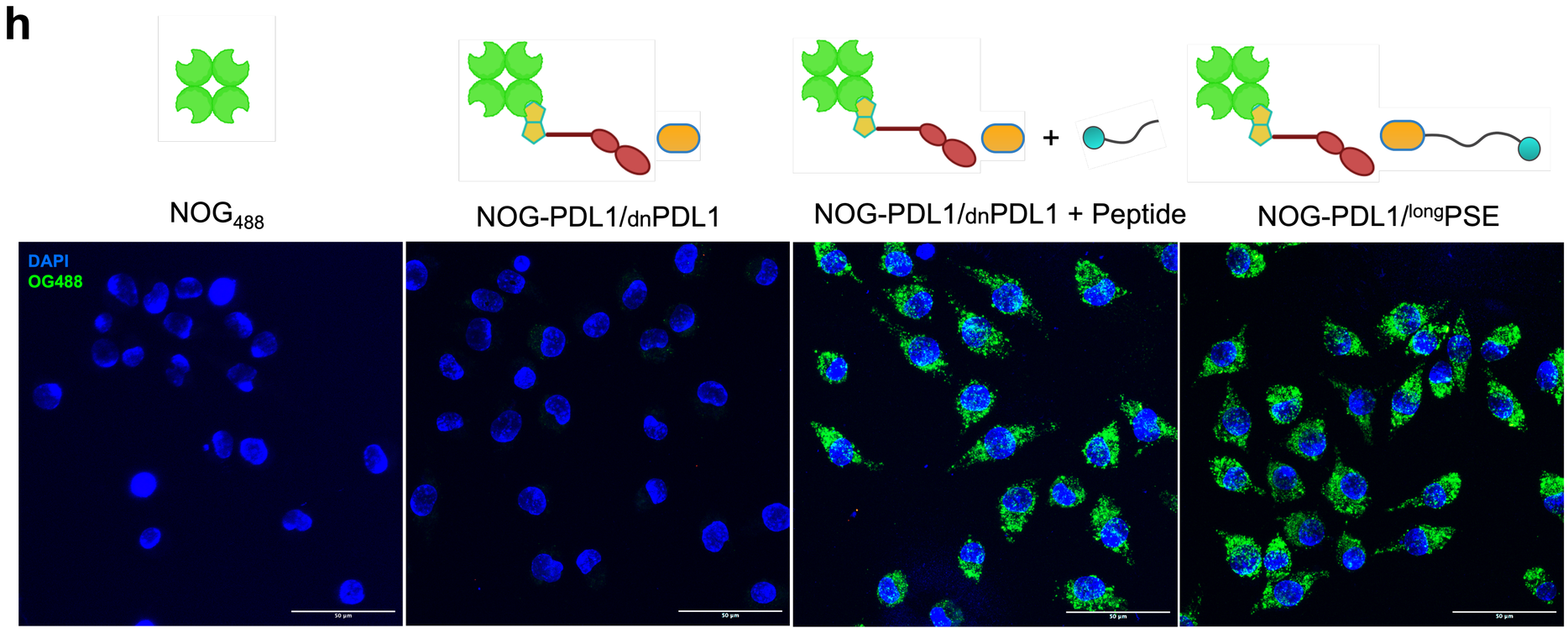

c
Normalized Frequency
Co-localized dyes
R1
Bright Detail Similarity FITC/Lysobrite
Co-localized dyes
R2
Bright Detail Similarity FITC/Lysobrite


d
Control
Peptide
dnPDL1
longPSE
MΦ surface PD-L1 (normalized)
****
***


e
Media
dnPDL1
longPSE
Lysosomal PD-L1 (%)
Co-localized Lysobrite+ APC+ MΦ


f
BF
Lysobrite
PD-L1
Merged
726
6181
2841
10 µm


g
PSE-mediated internalization of extracellular PD-L1
NOG-PDL1
longPSE
Macrophage
Internalization


h
NOG488
NOG-PDL1/dnPDL1
NOG-PDL1/dnPDL1 + Peptide
NOG-PDL1/longPSE
DAPI
OG488

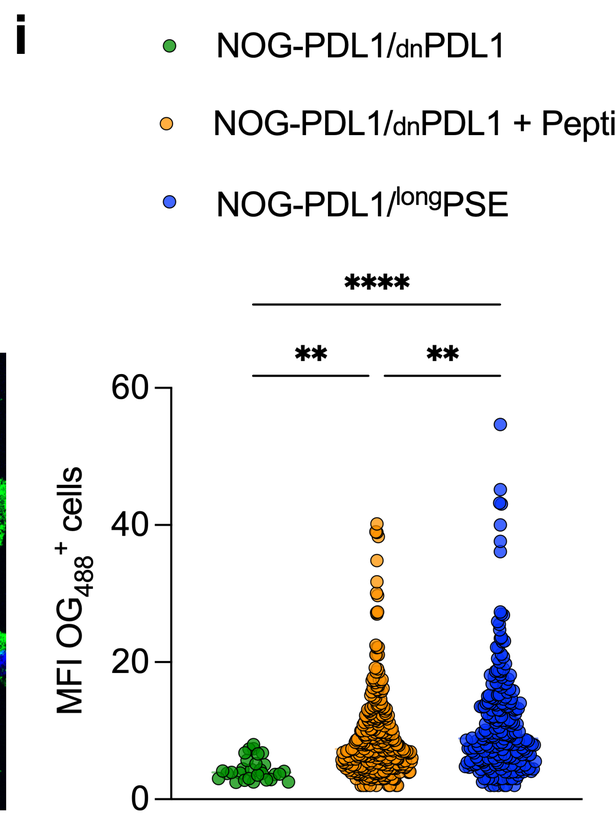
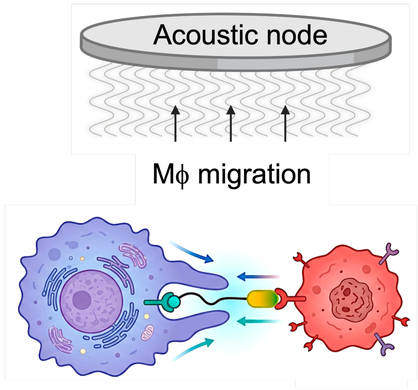
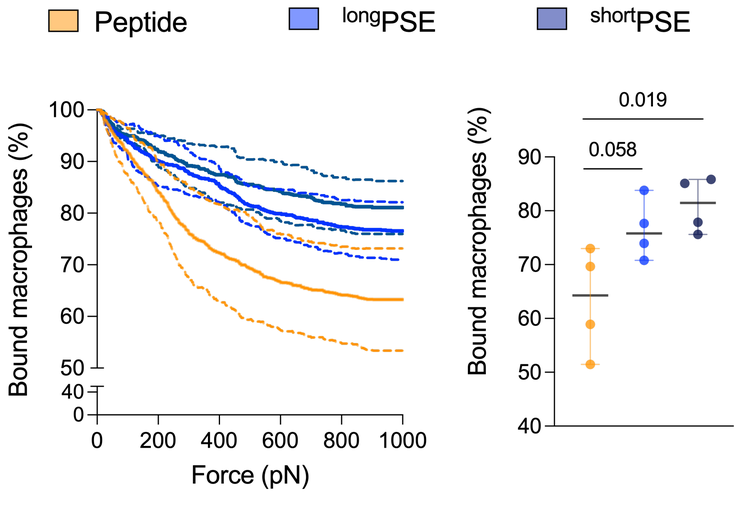
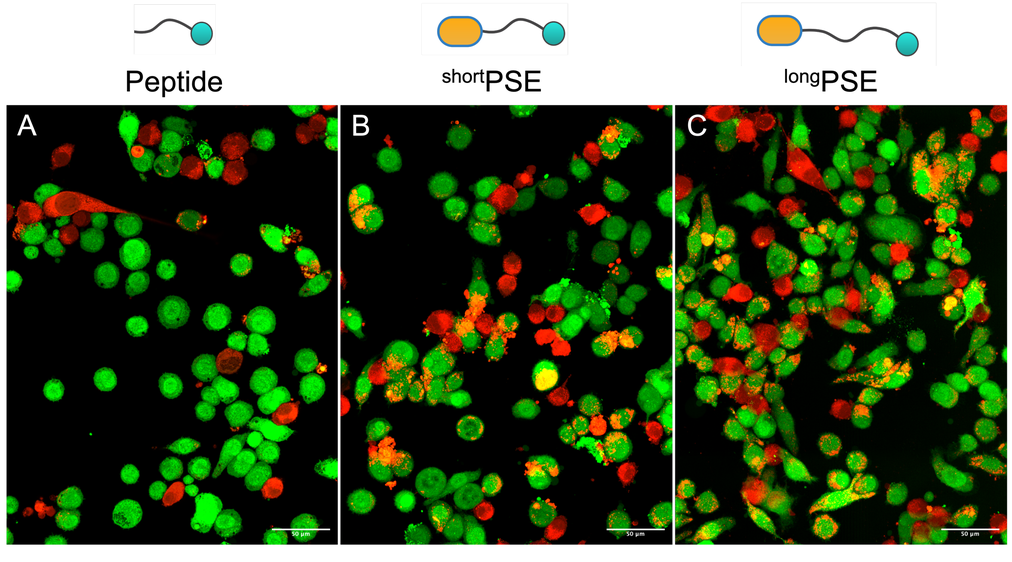
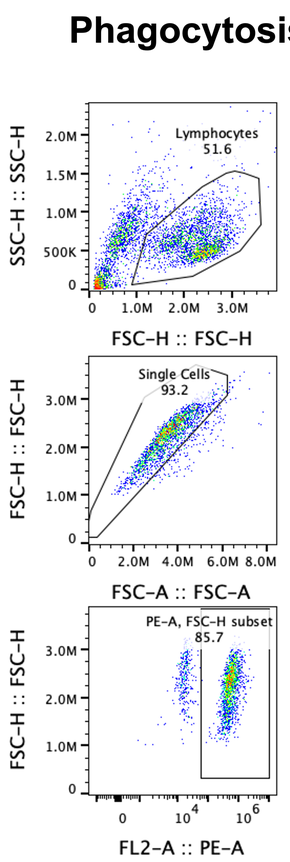

i
NOG-PDL1/dnPDL1
NOG-PDL1/dnPDL1 + Peptide
NOG-PDL1/longPSE
****
**
**
MFI OG488+ cells

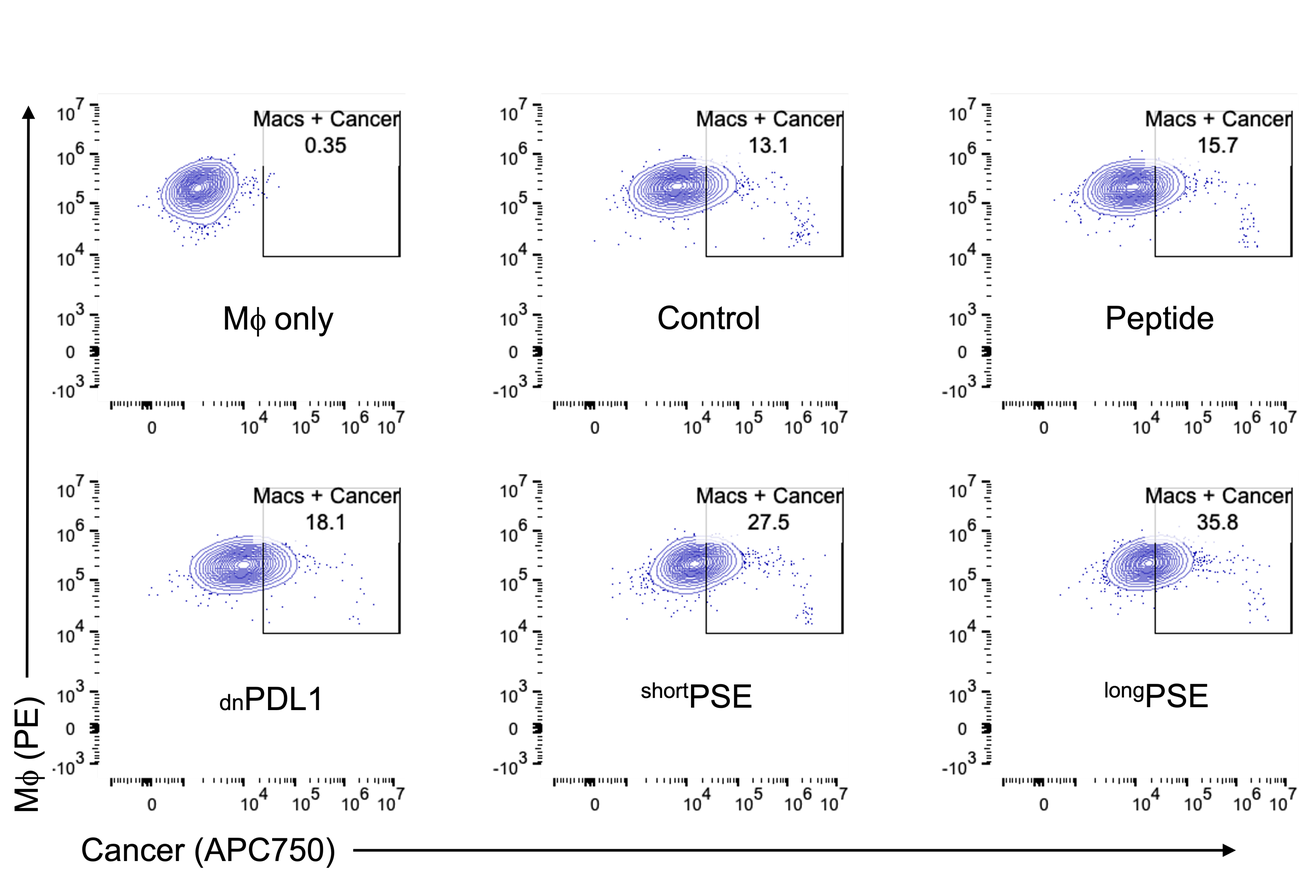
FIGURE 4

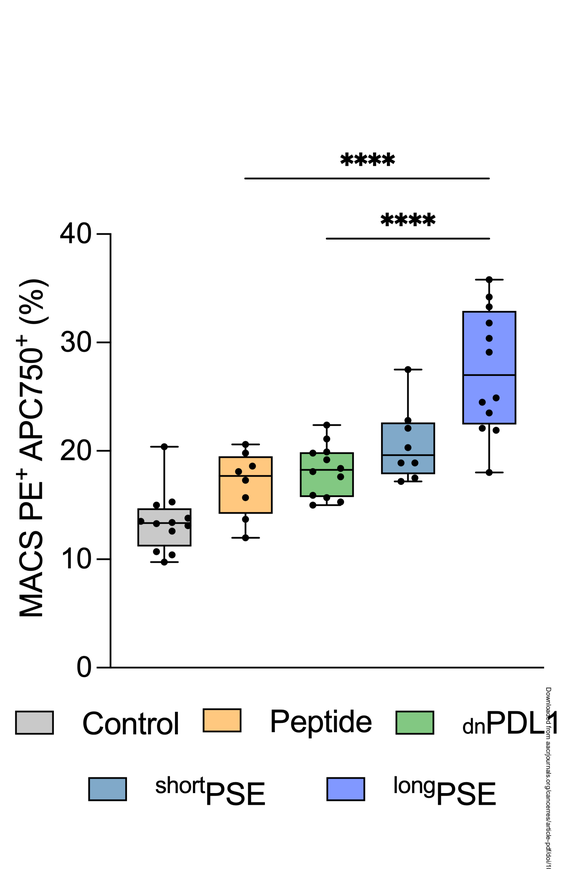

a
Avidity
Acoustic node
Mϕ migration

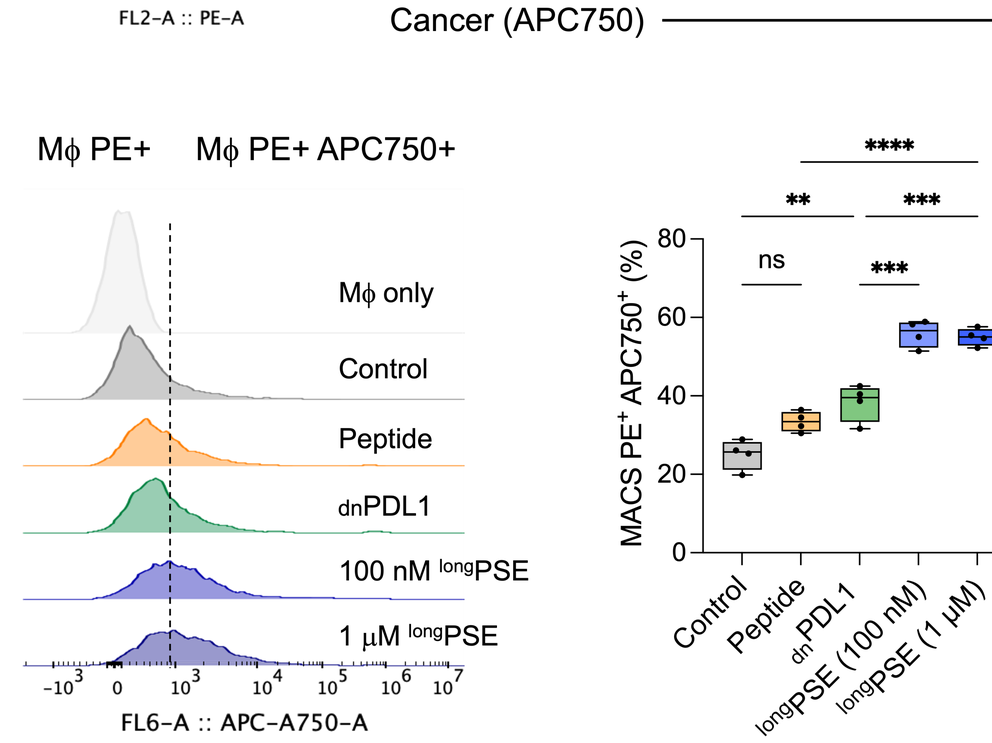

Peptide
longPSE
shortPSE
Bound macrophages (%)
Force (pN)
0.019
0.058

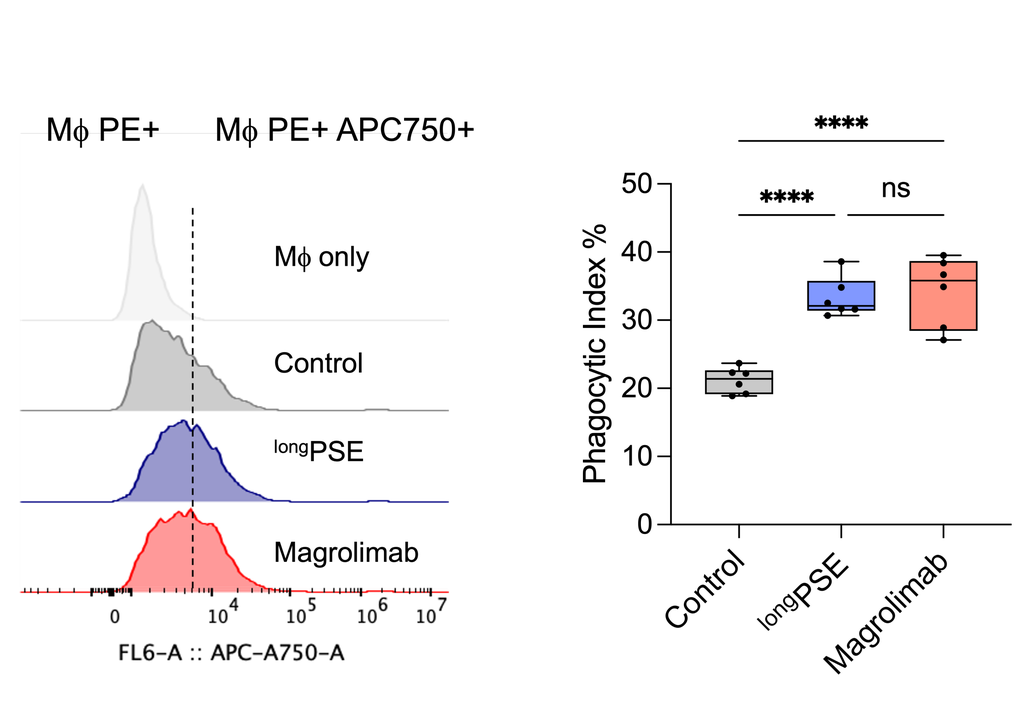

b
Peptide
shortPSE
longPSE
A
B
C

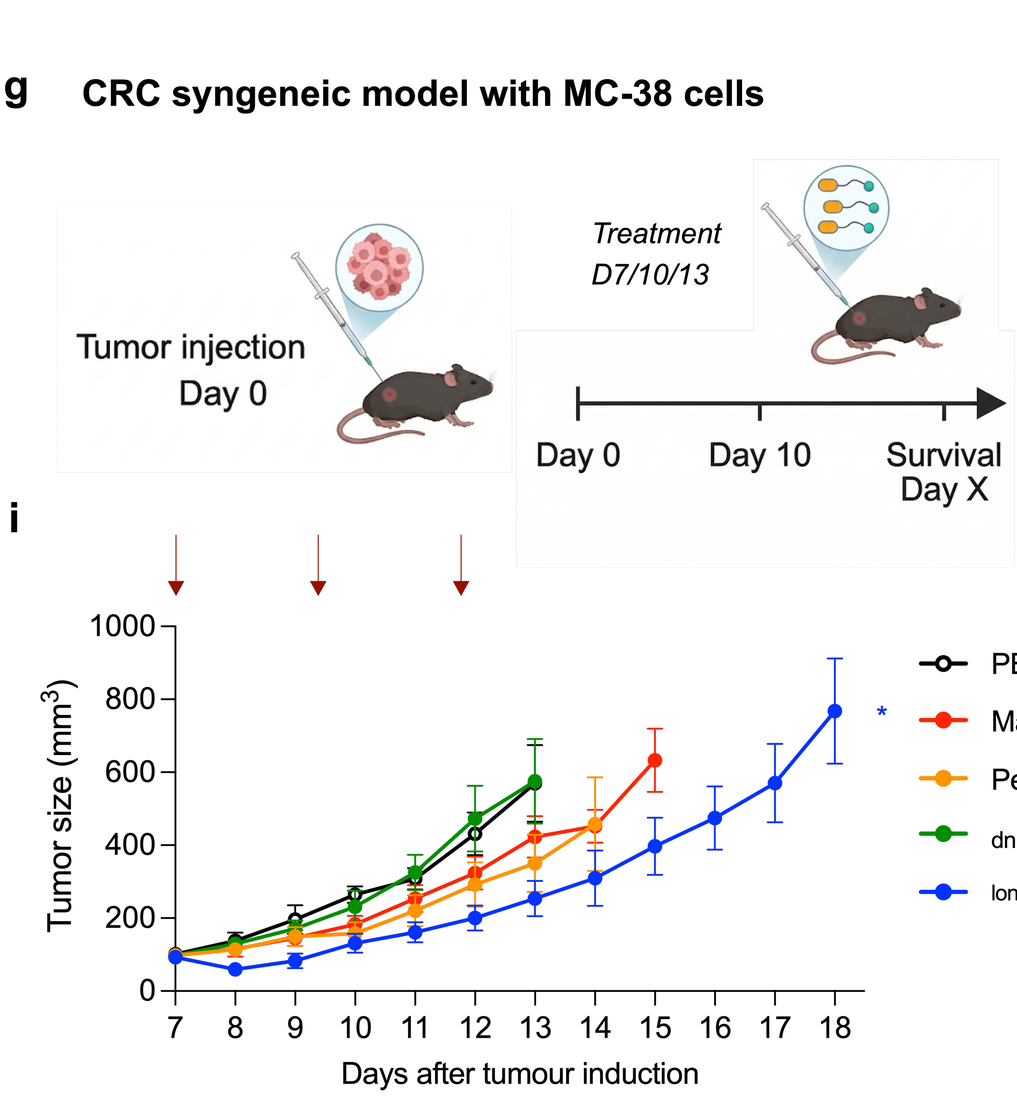

c
Phagocytosis
Lymphocytes
51.6
SSC-H :: SSC-H
FSC-H :: FSC-H
Single Cells
93.2
FSC-H :: FSC-H
FSC-A :: FSC-A
PE-A, FSC-H subset
85.7
FSC-H :: FSC-H
FL2-A :: PE-A

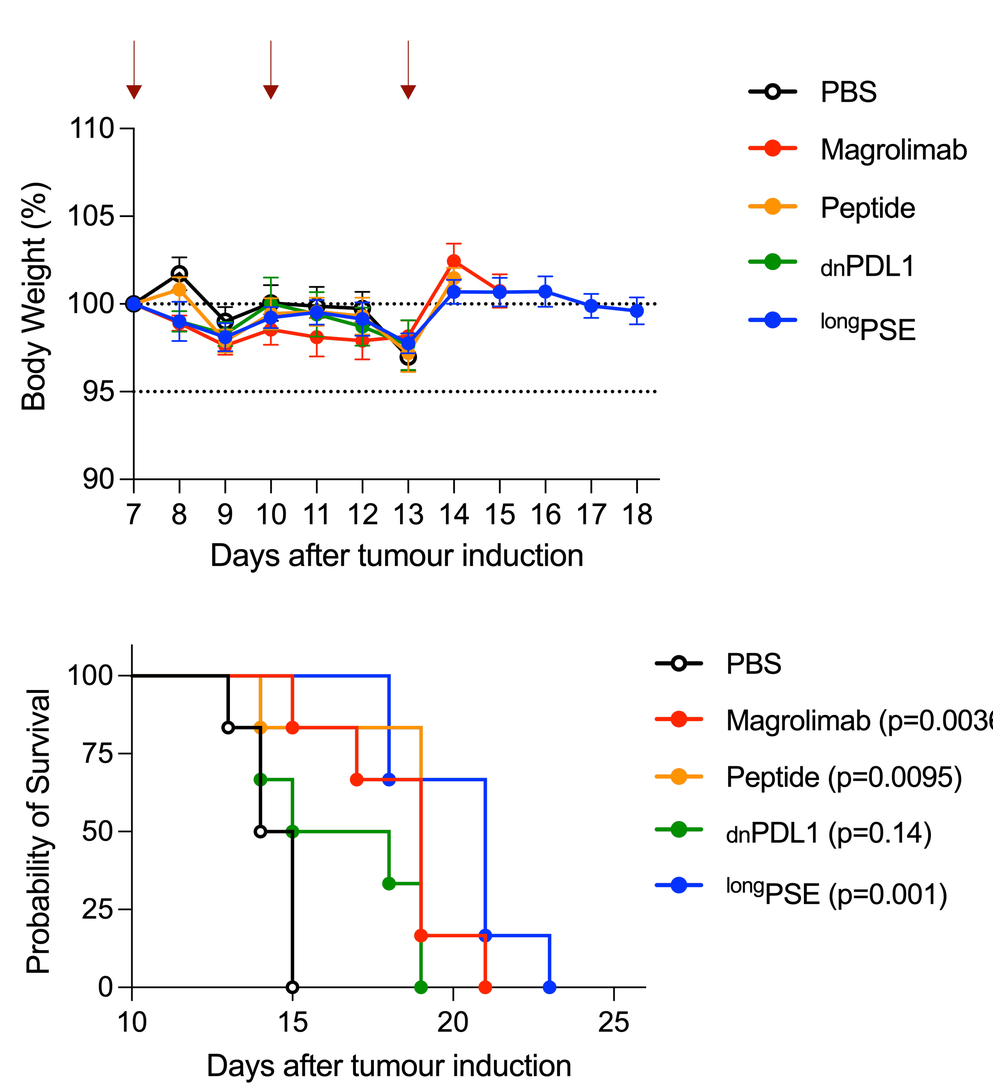

Macs + Cancer
0.35
Mϕ only
Macs + Cancer
13.1
Control
Macs + Cancer
15.7
Peptide
Macs + Cancer
18.1
dnPDL1
Macs + Cancer
27.5
shortPSE
Macs + Cancer
35.8
longPSE
Mϕ (PE)
Cancer (APC750)


d
****
****
MACS PE+ APC750+ (%)
Control
Peptide
dnPDL1
shortPSE
longPSE


e
Mϕ PE+
Mϕ PE+ APC750+
Mϕ only
Control
Peptide
dnPDL1
100 nM longPSE
1 μM longPSE
FL6-A :: APC-A750-A
****
**
***
***
ns
MACS PE+ APC750+ (%)
Control
Peptide
dnPDL1
longPSE (100 nM)
longPSE (1 μM)


f
Mϕ PE+
Mϕ PE+ APC750+
Mϕ only
Control
longPSE
Magrolimab
FL6-A :: APC-A750-A
****
****
ns
Phagocytic Index %
Control
longPSE
Magrolimab


g
CRC syngeneic model with MC-38 cells
Tumor injection
Day 0
Treatment
D7/10/13
Day 0
Day 10
Survival
Day X


h
PBS
Magrolimab
Peptide
dnPDL1
longPSE
Body Weight (%)
Days after tumour induction

i
Tumor size (mm3)
PBS
Magrolimab
Peptide
dnPDL1
longPSE
*
Days after tumour induction

j
Probability of Survival
PBS
Magrolimab (p=0.0036)
Peptide (p=0.0095)
dnPDL1 (p=0.14)
longPSE (p=0.001)
Days after tumour induction

FIGURE 5

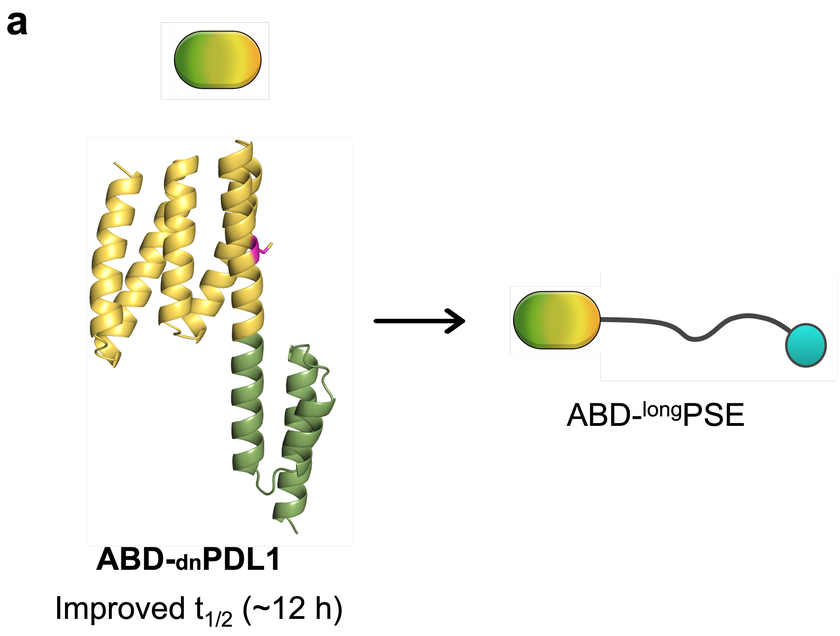
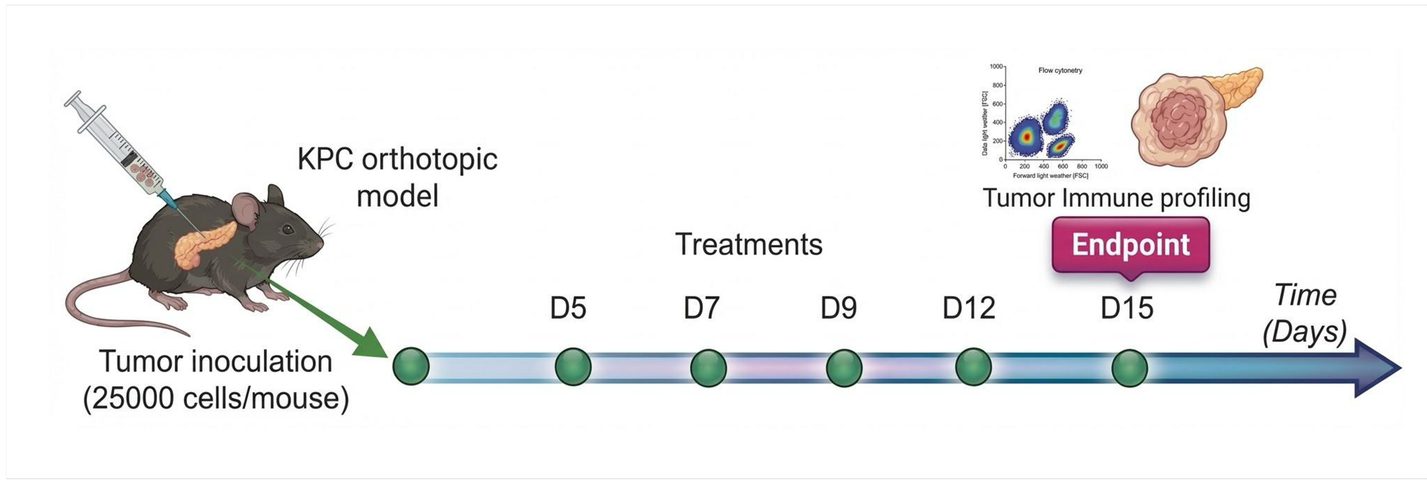

a
ABD-dnPDL1
Improved t1/2 (~12 h)
ABD-longPSE
b
kDa
250
130
100
70
55
35
25
15
10
1 2 3 4
1. ABD-dnPDL1
2. ABD-longPSE
3. dnPDL1
4. longPSE
c
dnPDL1
longPSE
ADB-dnPDL1
ABD-longPSE
Normalized % APC+ cells
Conc. (nM)
d
No Blockade (Inhibition)
TCR (T Cell Receptor)
Engineered TCR Activator
PD-1
PD-L1
PD-1 Effector Cell (Jurkat T cell)
PD-L1 aAPC/CHO-K1 Cell (Artificial Antigen Presenting Cell)
NFAT (Nuclear Factor of Activated T-cells)
Nucleus
Low Luciferase Expression
Luciferase Reporter Gene
NFAT-RE
Low Luminescence
Blockade (Activation)
Anti-PD-1 Antibody
or
Anti-PD-L1 Antibody
TCR Signaling
NFAT Activation
High Luciferase Expression
High Luminescence (Bio-Glo™ Substrate added)
e
Atezolizumab
ABD-longPSE
ABD-dnPDL1
Peptide
RLU
log10 (nM)
f
CRC model (i.t. injections)
Vehicle
Peptide
Magrolimab
dnPDL1
longPSE
ABD-dnPDL1
ABD-longPSE
i
Treatment
Body Weight (%)
Days after tumour induction
ii
Tumor size (mm3)
iii
Probability of Survival
g
CRC model (i.v. injections)
Vehicle
Peptide
ABD-dnPDL1
ABD-longPSE
Body Weight (%)
Tumor size (mm3)
Probability of Survival (%)
Days after tumour induction

FIGURE 6


a
KPC orthotopic model
Tumor inoculation (25000 cells/mouse)
Treatments
D5
D7
D9
D12
D15
Time (Days)
Flow cytometry
Tumor Immune profiling
Endpoint
b
Vehicle (PBS)
Magrolimab
ABD-dnPDL1
ABD-longPSE
Peptide
i
Fold change tumor burden
0.011
ii
Body weight change (% of initial weight)
Days after tumor inoculation
iii
Survival (%)
Days
***
c
i
% of CD45+ cells in live cells
0.066
0.005
ii
T cells (% of CD45+CD3+ live cells)
0.03
iii
Tregs (% of CD45+CD3+CD4+ CD25+FoxP3+ live cells)
0.037
0.005
0.021
iv
NK cells (% of CD45+NK1.1+ live cells)
0.056
0.042
v
CD4+ T cells (% of CD45+CD3+CD4+ live cells)
vi
CD8+ T cells (% of CD45+CD3+CD8+ live cells)
vii
PD-1+ CD4+T cells (% of CD45+CD3+CD4+PD-1+)
0.004
0.026
viii
PD-1+ CD8+T cells (% of CD45+CD3+CD8+PD-1+)
0.01
0.04
d
i
Neutrophiles & MDSCs (% of CD45+CD11b+LY6G+ live cells)
0.0005
ii
DCs (% of CD45+CD11b+CD11c+MHCII+ live cells)
iii
CD103+ DCs (% of CD45+CD11b+CD11c+ MHCII+CD103+ live cells)
0.015
iv
MFI PE-Dazzle594 PD-L1 (% of DC)
0.006
0.043
v
TAMs (% of CD45+CD11b+F4-80+)
0.001
0.008
vi
M2-like TAMs (% of CD45+CD11b+F4-80+CD206+ live cells)
0.012
0.007
vii
MFI PE-Dazzle594 PD-L1 (% of TAMs)
0.0007
0.0004
viii
MFI PE-Cy7 CD80 %CD45+Cd11b+F4/80+
0.002